AD-A110 482 GEORGIA INST OF TECH ATLANTA ENGINEERING EXPERIMENT --ETC F/G 21/2
THE KINETICS AND SPECTROSCOPY OF AIRCRAFT AND ROCKET PLUME CONS--ETC(U)
DEC 80 F P TULLY, A R RAVISHANKARA F49620-77-C-0011
UNCLASSIFIED AFOSR-TR-82-0624 NL

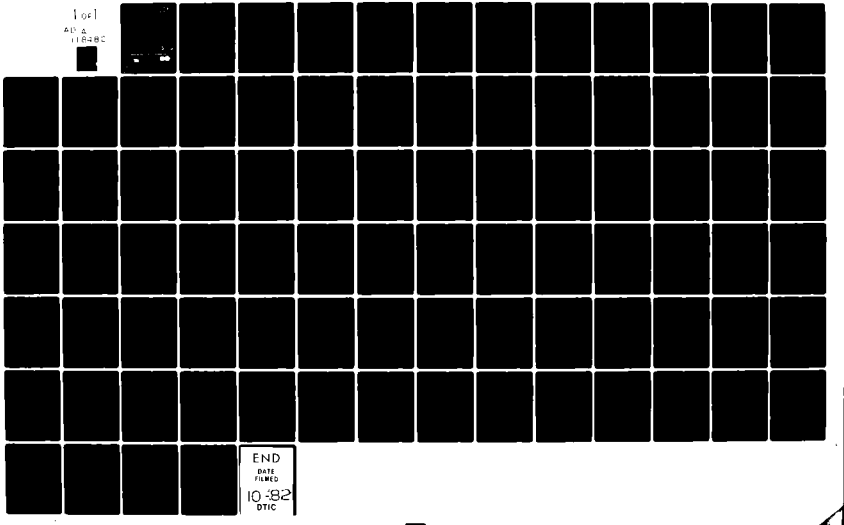

END
DATE FILMED
10-82
DTIC

THE KINETICS AND SPECTROSCOPY OF AIRCRAFT AND ROCKET PLUME CONSTITUENTS

By

F. P. Tully

A. R. Ravishankara

Prepared for:

Directorate of Aeromechanics and Energetics
Air Force Office of Scientific Research
Contract No. F49620–77–C–0111

FINAL TECHNICAL REPORT

GEORGIA INSTITUTE OF TECHNOLOGY
Engineering Experiment Station
Atlanta, Georgia 30332

UNCLASSIFIED

SECURITY CLASSIFICATION OF THIS PAGE (When Data Entered)

REPORT DOCUMENTATION PAGE		READ INSTRUCTIONS BEFORE COMPLETING FORM
1. REPORT NUMBER AFOSR-TR- 82-0624	2. GOVT ACCESSION NO. AD-A118482	3. RECIPIENT'S CATALOG NUMBER
4. TITLE (and Subtitle) KINETICS AND SPECTROSCOPY OF AIRCRAFT AND ROCKET PLUME CONSTITUENTS		5. TYPE OF REPORT & PERIOD COVERED 01 Jun 77 - 30 Sep 80 FINAL REPORT
		6. PERFORMING ORG. REPORT NUMBER
7. AUTHOR(s) F P TULLY A R RAVISHANKARA		8. CONTRACT OR GRANT NUMBER(s) F49620-77-C-0011
9. PERFORMING ORGANIZATION NAME AND ADDRESS GEORGIA INSTITUTE OF TECHNOLOGY ATLANTA, GEORGIA 30332		10. PROGRAM ELEMENT, PROJECT, TASK AREA & WORK UNIT NUMBERS 61102F 2308/A2
11. CONTROLLING OFFICE NAME AND ADDRESS Same as 14.		12. REPORT DATE 10 Dec 80
		13. NUMBER OF PAGES 78
14. MONITORING AGENCY NAME & ADDRESS (if different from Controlling Office) AIR FORCE OFFICE OF SCIENTIFIC RESEARCH/NA BOLLING AFB, DC 20332		15. SECURITY CLASS. (of this report) UNCLASSIFIED
		15a. DECLASSIFICATION/DOWNGRADING SCHEDULE

16. DISTRIBUTION STATEMENT (of this Report)

Approved for public release; distribution unlimited.

17. DISTRIBUTION STATEMENT (of the abstract entered in Block 20, if different from Report)

18. SUPPLEMENTARY NOTES

19. KEY WORDS (Continue on reverse side if necessary and identify by block number)

AIRCRAFT & ROCKET EXHAUST PLUMES
AIRBREATHING COMBUSTION
GLOBAL KINETICS
HYDROCARBON OXIDATION
ELEMENTARY CHEMICAL REACTIONS
OH RADICAL REACTIONS
HIGH TEMPERATURE KINETICS

20. ABSTRACT (Continue on reverse side if necessary and identify by block number)

During the course of this program experimental investigations were carried out to meet two objectives, (a) to measure the temperature dependence of rate coefficients of radical-molecule and molecule-molecule reactions of specific importance in modeling of combustion and plume processes, and (b) to contribute to the general understanding of the temperature dependence of bimolecular reactions, particularly as it relates to observed curvature in Arrhenius plots. The technique of flash photolysis-resonance fluorescence was adapted to measure directly rate coefficients for OH reactions in the temperature range of

DD FORM 1 JAN 73 1473 EDITION OF 1 NOV 65 IS OBSOLETE

UNCLASSIFIED

SECURITY CLASSIFICATION OF THIS PAGE (When Data Entered)

AIR FORCE OFFICE OF SCIENTIFIC RESEARCH
Contract No. F49620-77-C-0111

THE KINETICS AND SPECTROSCOPY OF AIRCRAFT AND ROCKET PLUME CONSTITUENTS

Final Scientific Report
June 1, 1977 - September 30, 1980

A-2009

By:

Molecular Sciences Branch
Physical Sciences Division
Electromagnetics Laboratory
Engineering Experiment Station
Georgia Institute of Technology
Atlanta, Georgia 30332

December 10, 1980

The research reported in this document has been sponsored by the Directorate of Aeromechanics and Energetics, The Air Force Office of Scientific Research, United States Air Force under Contract No. F49620-77-C-0111.

Table of Contents

ABSTRACT

During the course of this program experimental investigations have been carried out to meet two objectives, a) to measure the temperature dependence of rate coefficients of radical-molecule and molecule-molecule reactions of specific importance in modeling of combustion and plume processes, and b) to contribute to the general understanding of the temperature dependence of bimolecular reactions, particularly as it relates to observed curvature in Arrhenius plots. The technique of flash photolysis-resonance fluorescence has been adapted to measure directly rate coefficients for OH reactions in the temperature range of 250-1100 K. Kinetic data for the important reactions of OH + M_2, D_2, CH_4, C_2H_6, C_3H_8, HCl, and CO was obtained. In addition, the general oxidative conversion of BCl_3 and BF_3 were also investigated.

INTRODUCTION

Aircraft and rocket exhaust plumes provide an energetic, highly non-uniform, local environment within which microscopic physical and chemical processes act to dictate the nature of bulk observations of the medium. Analyses of fuel performance and tracking procedures rely on modeling of those contributing processes which, in combination, govern the efficiency of the propulsion system or surveillance method under examination. Chemically, reactions within the combustor and afterburning within the plume place heavy demands on the estimating prowess of kinetic modellers. In most cases, it is simply not possible to calculate which among the myriad of possible processes are most important (and thus which among the possible molecular species are of greatest concern)—an extensive data base, promoting realistic modeling parameter limitations, is needed. From a kinetic standpoint, optimized acquisition of this data base implies the measurement of oxidant/fuel/reaction intermediate reaction rate constants needed directly for model input and/or required as bases for the generation of 'global' kinetic equations applicable to entire families of chemical reactions. Improvement of the understanding of those factors which govern the temperature dependence of combustor/plume relevant bimolecular reactions was the primary goal of this research program.

The results are presented in the following four Sections. Section I has been recently published in the Journal of Physical Chemistry. Section III will be submitted shortly to the Journal of Physical Chemistry for publication. It is anticipated the contents of Section IV would also be submitted for publication in the next few months.

I. A FLASH PHOTOLYSIS-RESONANCE FLUORESCENCE KINETIC STUDY OF THE REACTIONS OH + H_2 → H_2O + H AND OH + CH_4 → H_2O + CH_3 FROM 298-1020 K

(Published in the Journal of Physical Chemistry, 84, 3126 (1980))

INTRODUCTION

Experimental measurements of absolute rate constants for radical-molecule reactions have historically been divided according to temperature regime. At low temperature ($T \lesssim 500K$) a variety of techniques[1] have been developed and utilized in recent years in response to the input demands of atmospheric chemical modeling. Generally speaking these techniques permit the adjustment of experimental conditions such that the absolute rate constant measurements for many specific radical-molecule reactions may be made with little, and/or quantifiable, interference from competing reaction processes. At high temperature ($T \gtrsim 1000K$) kinetic isolation of a given reaction has proven to be much more difficult to achieve. Experiments at flame temperatures typically range from studies utilizing end product analysis alone to investigations involving detailed concentration mapping vs. time (distance) of a number of radical (stable molecule) species whose interactive chemistry is very complex. Sequences of reaction schemes with parametrized absolute rate constant values are used to iteratively reproduce the measured concentration profiles (product yields). Frequently the extracted rate constants are model-dependent, ratioed to those of another insufficiently characterized reaction, or sensitive within only broad limits on the obtained raw data. The interpretive clarity of high temperature kinetic measurements has been observed to parallel the level of experimental control.

At temperatures intermediate between these separated regimes, 500-1000K, relatively few investigations of radical-molecule reaction rate constants have been undertaken. Two reactions which have received some attention[2,3] in this interval as well as extensive study at high and low temperatures are the subject of the present investigation:

$$OH + H_2 \xrightarrow{k_1} H_2O + H \qquad (1)$$

$$OH + CH_4 \xrightarrow{k_2} H_2O + CH_3 \qquad (2).$$

Published kinetic data on Reaction (1) has recently been critically evaluated and summarized by Cohen and Westberg.[4] Based principally on kinetic measurements made below 500K and above 1000K, these authors recommend a three-parameter rate constant expression of functional form $k(T) = AT^n \exp-(E_0/RT)$ as an appropriate fit to the Arrhenius graph curvature experimentally defined for Reaction (1). Non-Arrhenius behavior is also evident in kinetic measurements made on Reaction (2). Zellner[5] has used this same functional form to empirically effect a smooth joining of the low and high temperature rate constant measurements for this reaction.

In this paper we present the first in a series of studies of the reaction kinetics of the hydroxyl radical at intermediate temperatures. Using the direct kinetic technique of flash photolysis-resonance fluorescence absolute rate constants for Reactions (1) and (2) have been obtained up to temperatures of 1000K. These results will be described and compared with those of previous measurements and compilations.

EXPERIMENTAL SECTION

The application of the flash photolysis-resonance fluorescence technique to the study of OH radical reaction kinetics has been discussed previously.[6] Hence we will describe the experimental apparatus briefly, emphasizing only those new features which for the first time extend the temperature range of applicability of the technique to above 1000K.

A schematic diagram of the experimental apparatus is shown in Figure 1. The principal components of this system are (1) a quartz

reaction cell resistively heated using electrically insulated tantalum wire windings mounted to its graphite-coated outer surface; (2) a spark discharge flashlamp perpendicular to one face of the cell; (3) a CW OH resonance lamp perpendicular to the photolysis beam; (4) a photomultiplier/bandpass filter combination for monitoring OH resonance fluorescence perpendicular to both the photolysis and resonance radiation beams; and (5) a signal averager and fast photon counting electronics.

The present experiments were carried out using a static reactor configuration. Typical gas mixtures consisting of 150 mtorr H_2O, 0-1 torr $H_2(CH_4)$, and 50 Torr argon were flash photolyzed thereby initiating the primary reaction sequence

$$H_2O \xrightarrow[165\ nm\ <\ \lambda\ <185\ nm]{h\nu} H + OH(X^2\pi)$$

$$OH + H_2(CH_4) \xrightarrow{k_{bi}} H_2O + H(CH_3) .$$

It is worth noting here that our use of Suprasil quartz optics with a transmission cutoff at 165 nm prevented photolysis of H_2 and CH_4[7] and thus eliminated a major potential source of unwanted radicals and competing radical-radical reaction processes. Following the flash weakly focused resonance lamp radiation continuously excited a small fraction of the OH to the $A^2\Sigma^+$ state and the resultant (0,0) band fluorescence was counted in real time; the temporal profile of OH decay was constructed by signal averaging over a large number of flashes for each fixed reactant concentration. The reactant concentrations $[H_2]$ and $[CH_4]$ were maintained at large excess over [OH] ($[OH]_{t=0} \approx 1\text{-}5 \times 10^{11}$ molec/cm^3) and the reaction kinetics were thus pseudo first order in [OH]. Exponential [OH]$_T$ decays (through several 1/e times) were obtained, their time constants yielding the first order rate constant for OH disappearance at the re-

actant concentration of that mixture. Bimolecular rate constants were obtained as the slope of a plot of the measured first order rate constant vs. reactant concentration ([H_2] or [CH_4]). System parameters such as flash energy, H_2O concentration and total pressure were varied to demonstrate the lack of importance of competing secondary processes in our measurements on Reactions (1) and (2). During the generation of most [OH] decay curves several cycles of reactor filling/evacuation with identical gas mixtures were used so as to negate the kinetically deleterious effects of reactant depletion and product buildup (within the exposure limits used the measured rate constants were shown to be independent of the number of flashes to which any gas filling was subjected).

The two principal experimental factors which have permitted direct measurements of absolute rate constants to be made at temperatures in excess of 1000K involve the system optics configuration and the reaction cell design. Collimation and weak focusing of the incoming flashlamp and resonance lamp radiation and of the emitted fluorescence have been employed and have resulted in an OH detection sensitivity which is significantly enhanced relative to that available in previous high-pressure studies of Reactions (1) and (2). A detailed discussion of the detection sensitivity characteristics of a completely analogous experimental configuration is contained in a recent publication[8] describing our laboratory's study of the $OH + NO_2 + M \rightarrow HNO_3 + M$ reaction. Highly polished Suprasil windows have been fused using quartz tape to an all quartz body to form the high-temperature reactor.[9] Efficient heating and radiation shielding maintain a higher temperature at the body of the reactor than that at the protruding windows, the reaction temperature being measured by both internal (insertable) and external (body-

mounted) Chromel-Alumel thermocouples. During the period of measurement of each individual bimolecular rate constant the reactor temperature was held constant to within ± 3K by applying a controlled constant voltage to the resistive heaters. The temperature profile along the axis of the cylindrical reactor was measured using the retractable thermocouple at pressure conditions identical to those existing during kinetic measurements. The temperature differential between the upper and lower portions of the reaction zone (maximum length $\lesssim$ 2 cm) was found to be $\leq$ 5K at a reactor temperature of 1000K. The bottom window (fluorescence port) temperature was measured to be $\approx$ 25K below that of the reaction zone at 1000K; given the heater and radiation shield positions and the overall reactor geometry, side window temperatures are estimated to be comparable to that measured at the bottom window. Considering the relatively large reactor diameter used in this work (reactor volume $\approx$ 500 cm^3), such temperature gradients are likely to be only a minimal source of experimental error.

Figure 2 shows typical OH decay profiles at three temperatures. These decay rates were all measured using the same diluent gas pressure, H_2O pressure, and photolysis flux. The high temperature experiments required longer periods of signal averaging than the lower temperature measurements; for example, twice as many flashes were needed at 1020K than at 619K to produce a good quality decay curve. At an H_2O partial pressure of $\sim$ 150 mTorr the fluorescence signal strength as a function of temperature was seen to scale closely with H_2O number density indicating minimal temperature dependent optics transmission effects; repeated temperature cycling of the reactor did, however, induce long-term degradation of the vacuum-UV transmission efficiency of the Suprasil windows.

[The static reactor used in the present work has since been replaced by an analogous "slow flow" high-temperature quartz reaction cell which transmits a continuously controlled flow of mixture of desired composition and thereby permits each initiating flash to encounter a "locally fresh" reaction mixture.]

The gases used in this study were obtained from Matheson Co. and had stated minimum purities as follows: H_2, 99.9999%; CH_4, 99.99%; and Ar, 99.9995%. Prior to their use, hydrogen and methane were passed through a trap at 77K to remove residual condensibles.

RESULTS AND DISCUSSION

The bimolecular reaction rate constants obtained in this study were generated from measurements of hydroxyl radical decay rates at several fixed reactant concentrations for each temperature. Plots of the first order decay constant vs. reactant concentration at selected temperatures between 499-1020 K are given for Reactions (1) and (2) in Figures 3 and 4, respectively. The bimolecular rate constants obtained as the slopes of the included least-square lines are listed with $\pm 2\sigma$ precision limits in Tables I and II. Room temperature rate constant values obtained in this work are in good agreement with those of previous studies tabulated in the data evaluations of References 4 and 5.

The major potential sources of systematic error in the measured values of k_1 and k_2 are the uncertainties in the reactant concentrations and in the temperature. At 298K the reactant concentrations of source mixtures could be determined quite accurately ($\lesssim$ 3%) using a capacitance manometer since both H_2 and CH_4 are non-sticky and non-condensible compounds. Reaction fillings were made using these calibrated source mixtures and elevated temperature reactant concentrations were calculated by scal-

ing accordingly to source mixture content and temperature. Including errors due to temperature uncertainties, then, the estimated error in reactant concentrations was $\leq$ 10%. Thus we estimate that the accuracies (95% confidence limit) of the measured values of k_1 and k_2 are $\sim$ 13% at 298K increasing to $\sim$ 20% at 1000K.

Our data for $k_1(T)$ are plotted along with selected previous results and analytical evaluations in Arrhenius graph form, $\ell n\ k(T)$ vs. 1000/T, in Figure 5. Our results cover a sufficiently wide temperature range to independently demonstrate the existence of curvature in the Arrhenius plot for Reaction (1). At low and relatively high temperature our measurements are in excellent agreement with the rate constant values calculated from Cohen and Westberg's summary expression[4] $k_1(T) = 1.83 \times 10^{-15}\ T^{1.3}$ $\exp(-1835/T)$ $cm^3 molec^{-1} sec^{-1}$. In the interval 499-648 K, however, measurements made in the present study fall about 20% below those derived from this $k_1(T)$ expression. Similarly, in the only previously published direct kinetic study of Reaction (1) at intermediate temperatures, Westenberg and deHaas[2] measured k_1 values between 403-745 K which averagd 22% below those calculated from the Cohen and Westberg formula. Interestingly Cohen and Westberg did not weight data at intermediate temperatures heavily in their evaluation; indeed, hardly any measurements between 500-1000 K were available. While our measurements yield generally very good agreement with the $k_1(T)$ values calculated from Cohen and Westberg's expression, they do suggest somewhat more pronounced Arrhenius graph curvature than that expression describes. The best fit expression calculated from our data only is $k_1(T) = 4.12 \times 10^{-19}\ T^{2.44}\ \exp(-1281/T)$ $cm^3 molec^{-1} sec^{-1}$. Zellner's suggested[5] expression of $k_1(T) = 1.66 \times 10^{-15}\ T^{1.6}\ \exp(-1660/T)$ $cm^3 molec^{-1} sec^{-1}$ is perhaps the most appropriate fit to all available data. [With regard to curvature in Arrhenius plots it is of interest to note that preliminary

results of our OH + D_2 → DHO + D study[10] between 298-932 K demonstrate markedly less Arrhenius graph curvature than that found to be appropriate for Reaction (1).]

Our rate constant measurements for the $OH + CH_4 \xrightarrow{k_2} H_2O + CH_3$ (2) reaction are plotted along with selected previous work in Arrhenius graph form in Figure 6. Once again our data clearly demonstrates the existence of pronounced Arrhenius graph curvature for Reaction (2). Immediately apparent from this figure is the fact that straight-line extrapolations of either the low-temperature based NASA recommendation[11] or the high-temperature based Peeters and Mahnen recommendation[12] produce order of magnitude errors in $k_2(T)$ in the opposite temperature regime. Based principally on low- and high-temperature experimental measurements, Zellner[5] derived an emiprical best fit for $k_2(T)$ given by $k_2(T) = 2.57 \times 10^{-18} T^{2.13} \exp(-1233/T)$ $cm^3 molecule^{-1} sec^{-1}$. Within experimental error both our data (298-1020 K) and the single point of Ernst, Wagner and Zellner (1300k)[13] fall dead-on the curve (solid line in Figure 6) traced out by this expression. Interestingly, the calculated best fit expression based on our data only, $k_2(T) = 1.32 \times 10^{-17} T^{1.92} \exp(-1355/T)$ $cm^3 molec^{-1} sec^{-1}$, yields a curve which is barely distinguishable from that recommended by Zellner. Indeed, given the quoted accuracies of these and previous measurements on Reaction (2), a rather extended array of parameters could be suggested as producing representative fits for $k_2(T)$. While the present experiments have demonstrated both the appropriateness of the functional form $k(T) = AT^n \exp(-Eo/RT)$ and the basic soundness of previous measurements in each separated temperature regime, the curve fitting calculations indicate that extreme caution must be exercised when attaching physical significance to multi-parameterized rate constant expressions.

At intermediate temperatures only one prior direct kinetic investigation of Reaction (2) has been undertaken. Using the technique of flash photolysis-resonance absorption, Zellner and Steinert[3] measured $k_2(T)$ up to temperatures of 892K. At lower temperatures these data agree well with Zellner's empirical fit, but at higher temperatures their measured $k_2(T)$ values exceed the best fit values by a factor increasing with temperature and already more than two at 892K.

One possible explanation for the discrepancy at higher temperatures between Zellner and Steinert's results and those of the present study relates to the magnitude of the hydroxyl radical reactant concentration demanded by the resonance absorption and fluorescence detection modes. Although both techniques measure the disappearance of OH radicals in real time, the absorption technique monitors the difference between two large numbers $[(I_{t=0} - I_t)/I_{t=0}]$ and thereby requires much larger OH concentrations to match the statistics obtainable from the fluorescence technique. Thus Zellner and Steinert's initial post-flash OH concentrations were 40-100 times higher and their $[CH_4]/[OH]_{t=0}$ ratios were $\sim$ 10 times lower than those characteristic of the present study. Such larger radical concentrations and lower reactant ratios enhance the probability of OH disappearance due to processes other than Reaction (2) and make more difficult kinetic isolation of this subject reaction. Based on sensitivity considerations, then, it appears that the fluorescence detection technique is best suited to the investigation of intermediate temperature hydroxyl radical reaction kinetics; indeed, it is the authors' opinion that present constraints on the general applicability of the flash photolysis-resonance fluorescence technique to combustion regime kinetics of O, H, and OH relate more to maintenance of the mechanical and optical

integrity of the experimental system than to limitations in detection sensitivity.

The experiments described above represent the first use of the flash photolysis-resonance fluorescence technique in the study of radical-molecule reaction kinetics above 500K. The need for direct kinetic investigations of prototype radical-molecule reactions from low temperatures to those well within the flame region is indisputable. Combustion modeling requires voluminous rate constant input from both direct measurement and extrapolation [note here the improvement in extrapolative accuracy achievable upon progression of data availability limits from 400K (1000/T = 2.5) to 1000K (1000/T = 1.0)]. Enhancement of our general understanding of bimolecular reaction rate theory is ultimately required to render practical the global kinetic approach to the chemical modeling of complex systems. Unambiguous rate constant studies over wide temperature ranges ($0.5 \leq 1000/T \leq 5.0$) will promote this goal.

ACKNOWLEDGEMENT

This work was supported by the Air Force Office of Scientific Research under Contract No. F49620-77-C-0111. Early stages of the apparatus development phase of this work were supported by the National Bureau of Standards through Grant No. GT-9020.

REFERENCES

1. (a) C. J. Howard, J. Phys. Chem. 83, 3(1979);
   (b) J. V. Michael and J. H. Lee, J. Phys. Chem. 83, 10(1979);
   (c) F. Kaufman, Ann. Rev. Phys. Chem. 30, 411(1979), and references therein.

2. A. A. Westenberg and N. deHaas, J. Chem. Phys. 58, 4061(1973).

3. R. Zellner and W. Steinert, Int. J. Chem. Kinet. 8, 397(1976).

4. N. Cohen and K. Westberg, J. Phys. Chem. 83, 46(1979).

5. R. Zellner, J. Phys. Chem. 83, 18(1979).

6. (a) D. D. Davis, S. Fischer, and R. Schiff, J. Chem. Phys. 59, 628(1974);
   (b) A. R. Ravishankara, P. H. Wine, and A. O. Langford, J. Chem. Phys. 70, 984(1979), and references therein.

7. J. G. Calvert and J. N. Pitts, Jr., Photochemistry, John Wiley and Sons, Inc., 1966.

8. P. H. Wine, N. M. Kreutter, and A. R. Ravishankara, J. Phys. Chem. 83 3191(1979).

9. The reactor was fabricated by R and D Opticals Inc., New Windsor, Maryland.

10. A. R. Ravishankara, R. C. Shah, J. M. Nicovich, R. L. Thompson, and F. P. Tully, work in progress.

11. R. D. Hudson and E. I. Reed, The Stratosphere: Present and Future, NASA Reference Publication 1049, December 1979.

12. J. Peeters and G. Mahnen, 14th Symp. (Int.) Combustion, The Combustion Institute, p. 133 (1973).

13. J. Ernst, H. Gg. Wagner, and R. Zellner, Ber. Bunsenges. Phys. Chem. 82, 409(1978).

Table I.

Bimolecular Rate Constant vs. Temperature
for Reaction (1): $OH + H_2 \rightarrow H_2O + H$

Temperature	$k_{bimolecular}$ ($cm^3 molec^{-1} sec^{-1}$)
298	$(6.08 \pm 0.37) \times 10^{-15}$
499	$(1.15 \pm 0.08) \times 10^{-13}$
576	$(2.34 \pm 0.18) \times 10^{-13}$
648	$(3.84 \pm 0.18) \times 10^{-13}$
739	$(7.64 \pm 0.56) \times 10^{-13}$
838	$(1.30 \pm 0.10) \times 10^{-12}$
904	$(1.86 \pm 0.35) \times 10^{-12}$
992	$(1.99 \pm 0.19) \times 10^{-12}$

*Stated Error Bounds Represent the 2σ Values

Table II.

Bimolecular Rate Constant vs. Temperature
for Reaction (2): $OH + CH_4 \rightarrow H_2O + CH_3$

Temperature	$k_{bimolecular}$* ($cm^3 molec^{-1} sec^{-1}$)
298	$(7.50 \pm 0.60) \times 10^{-15}$
398	$(4.73 \pm 0.45) \times 10^{-14}$
448	$(8.1 \pm 1.1) \times 10^{-14}$
511	$(1.45 \pm 0.12) \times 10^{-13}$
529	$(1.67 \pm 0.06) \times 10^{-13}$
600	$(3.14 \pm 0.40) \times 10^{-13}$
619	$(2.75 \pm 0.44) \times 10^{-13}$
696	$(5.78 \pm 0.58) \times 10^{-13}$
772	$(8.4 \pm 1.5) \times 10^{-13}$
915	$(1.50 \pm 0.15) \times 10^{-12}$
1020	$(2.00 \pm 0.20) \times 10^{-12}$

*Stated Error Bounds Represent the 2σ Values

FIGURE CAPTIONS

Fig. 1. Schematic drawing of the experimental apparatus. (For clarity the flashlamp and resonance lamp are pictured at 180° to each other whereas in reality they were situated at 90°).

Fig. 2. Typical OH temporal profiles observed following flash photolysis of H_2O/CH_4/diluent mixtures. Experimental conditions: P = 50 Torr, diluent = Ar, flash energy = 120 J, H_2O pressure = 150 mTorr. The concentrations of methane, temperature, and the number of traces averaged are shown next to each line.

Fig. 3. Plot of the first order rate constant versus the H_2 concentration for Reaction (1) at several temperatures.

Fig. 4. Plot of the first order rate constant versus the CH_4 concentration for Reaction (2) at several temperatures.

Fig. 5. Arrhenius graph for Reaction (1).

Fig. 6. Arrhenius graph for Reaction (2).

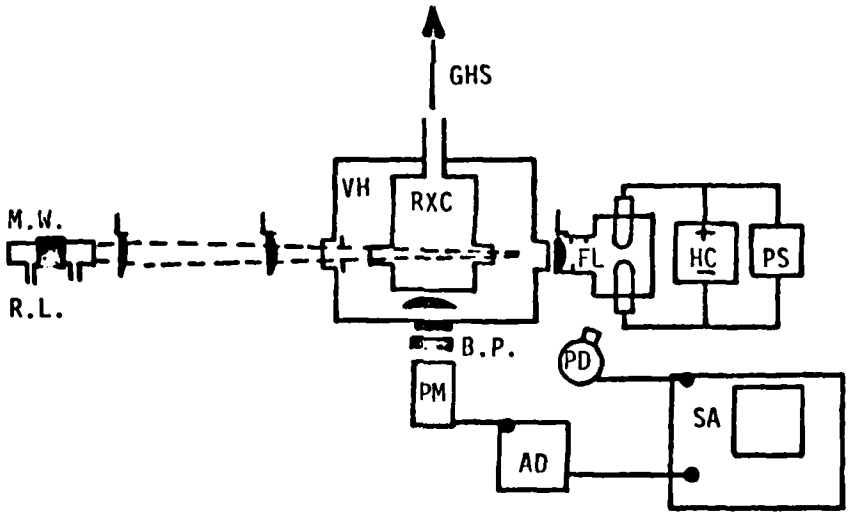

AD: AMPLIFIER/DISCRIMINATOR
B.P.: BANDPASS FILTER
FL: FLASHLAMP
GHS: GAS HANDLING SYSTEM
HC: HIGH VOLTAGE CAPACITOR
L: LENS
M.W.: MICROWAVE CAVITY (Evenson Type)
PD: PHOTODIODE
PM: PHOTOMULTIPLIER
PS: POWER SUPPLY
R.L.: RESONANCE LAMP
RXC: REACTION CELL
VH: VACUUM HOUSING
SA: SIGNAL AVERAGER

Figure 1.

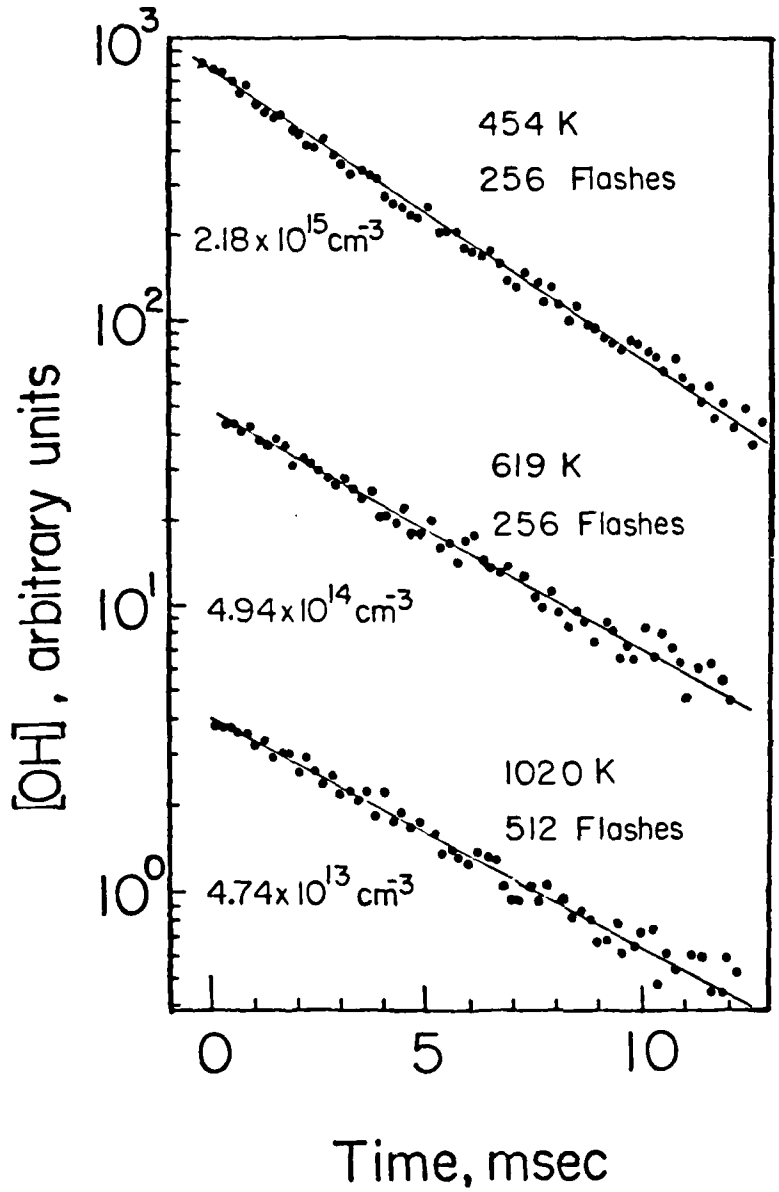
454 K
256 Flashes
2.18 x 10^15 cm^-3
619 K
256 Flashes
4.94x10^14 cm^-3
1020 K
512 Flashes
4.74x10^13 cm^-3
10^3
10^2
10^1
10^0
[OH], arbitrary units
0
5
10
Time, msec

Figure 2.

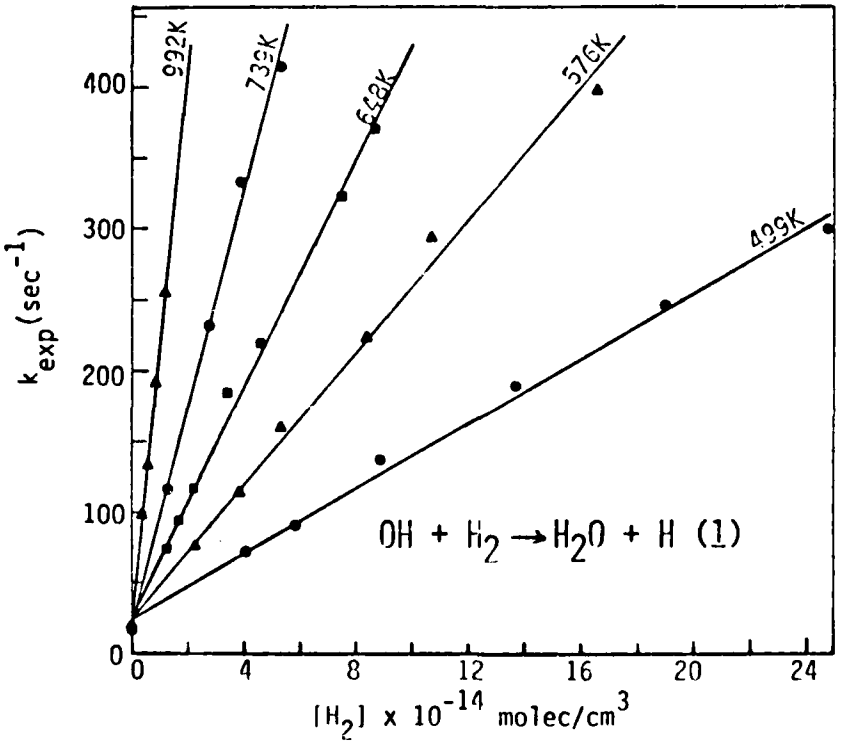
992K
733K
648K
576K
499K
400
300
200
100
0
$k_{exp}(sec^{-1})$
OH + H_2 → H_2O + H (1)
0
4
8
12
16
20
24
$[H_2] \times 10^{-14}$ molec/cm^3

Figure 3.

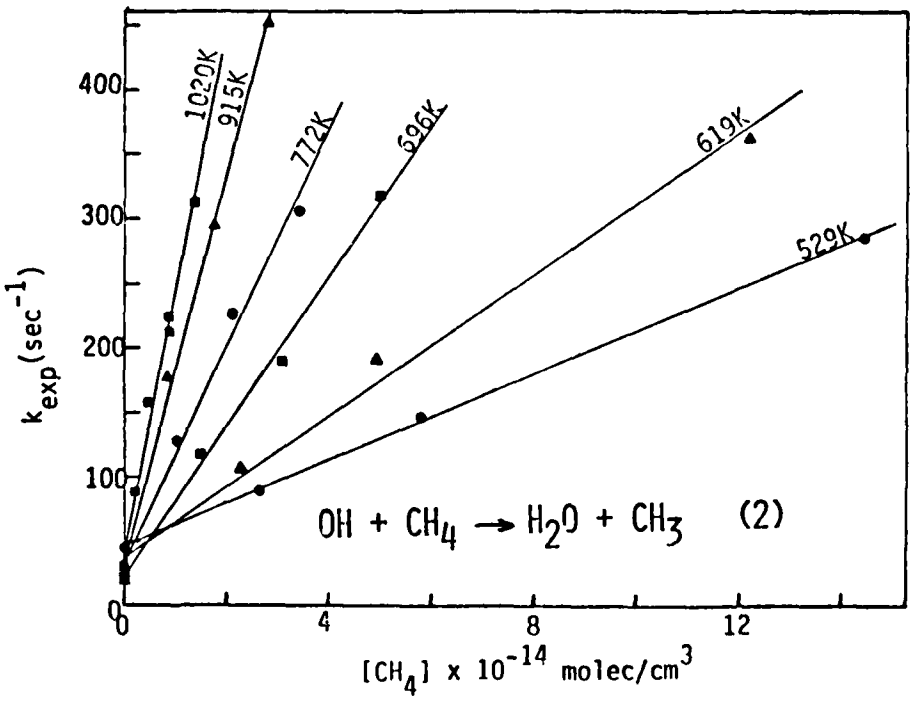
400
300
200
100
0
0
4
8
12
$k_{exp}(sec^{-1})$
$[CH_4] \times 10^{-14}$ molec/cm^3
1020K
915K
772K
696K
619K
529K
OH + CH_4 → H_2O + CH_3 (2)

Figure 4.

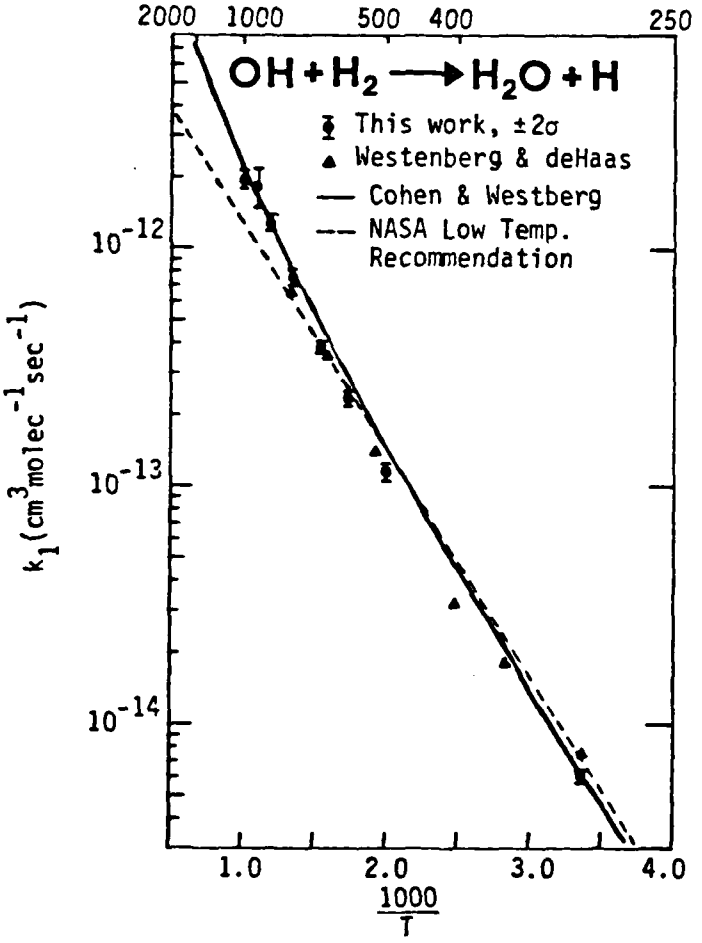
2000
1000
500
400
250
OH + H2 → H2O + H
This work, ±2σ
Westenberg & deHaas
Cohen & Westberg
NASA Low Temp. Recommendation
10-12
10-13
10-14
k1(cm3molec-1sec-1)
1.0
2.0
3.0
4.0
1000/T

Figure 5.

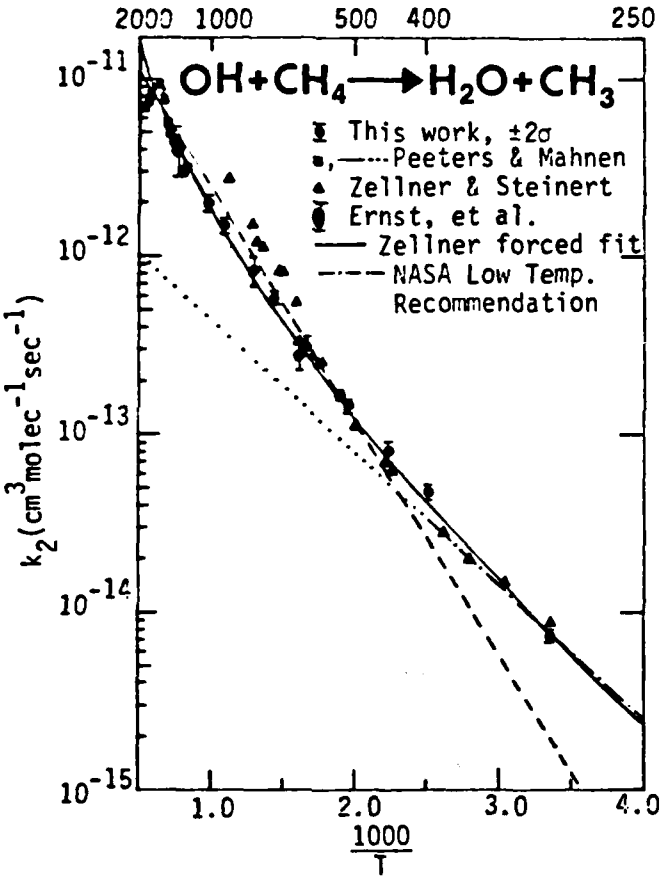
2000 1000 500 400 250
OH+CH4 → H2O+CH3
This work, ±2σ
Peeters & Mahnen
Zellner & Steinert
Ernst, et al.
Zellner forced fit
NASA Low Temp. Recommendation
10-11
10-12
10-13
10-14
10-15
k2(cm3molec-1sec-1)
1.0
2.0
3.0
4.0
1000/T

Figure 6.

II. OXIDANT-HALOCARBON STUDIES

The achievement of an understanding of the oxidation characteristics of halogenated boron species is essential to the estimation of the concentrations of boron molecular emitters present in advanced fuel rocket plume exhausts. Knowledge of the typical concentrations of emitting species is a prerequisite to the interpretation of rocket plume infrared signatures. Since very little is known about haloborane oxidation (and also about the technology required for its study), we have studied relevant molecular reactions with the aim of aiding development of experimental techniques which would permit future investigation of the more complex radical reactive systems.

In the work statement for this program we were contracted to measure absolute rate constants for Reactions (1) and (2),

$$O_2 + BF_3 \rightarrow \text{Products} \qquad (1)$$

$$O_2 + BCl_3 \rightarrow \text{Products}, \qquad (2)$$

using the technique of stop-flow time-of-flight mass spectrometry. A schematic diagram of this technique is displayed in Figure 1. In this system a thermostated reaction vessel equipped with a very small molecular leak is positioned directly above the ion source of a time-of-flight mass spectrometer. Reactants are admitted to the vessel and mix homogeneously and reach temperature equilibrium within a few milliseconds. Following mixing, the reaction is occurring at the desired conditions of temperature, pressure and reactor composition. The molecular leak at the bottom of the reaction cell allows a very small fraction of the cell contents to diffuse into the ion source of the mass spectrometer. This effluent is ionized, the ions are accelerated to constant energy, and the ion current and time of

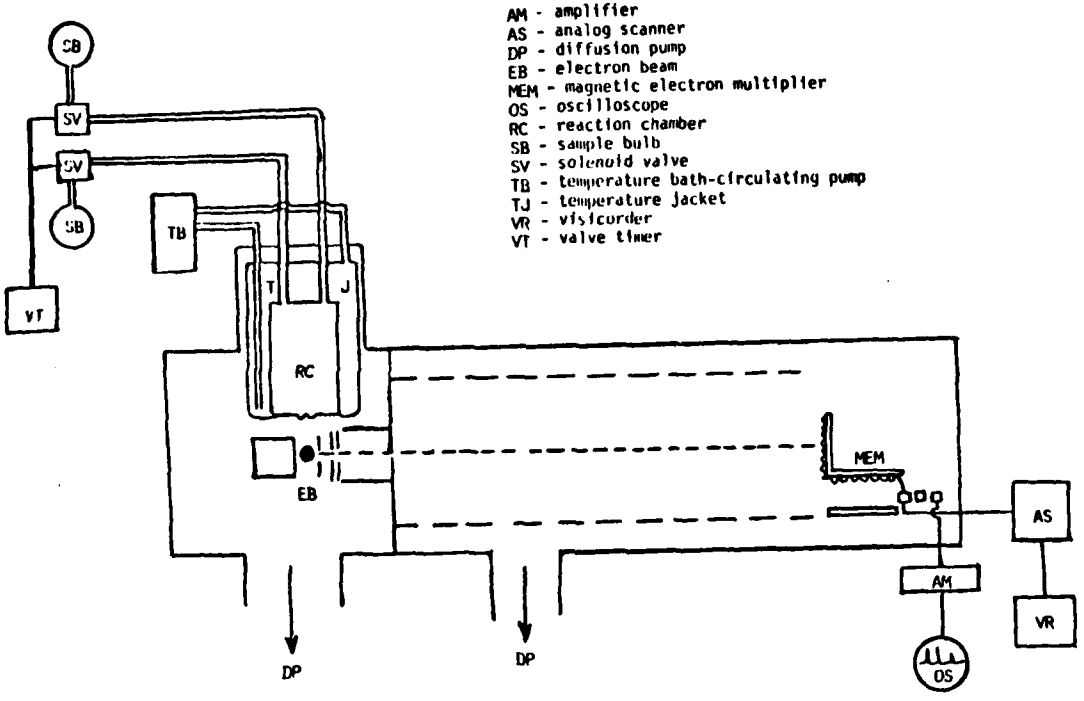

Figure 1. Stop-Flow Time-of-Flight Mass Spectrometer System.

arrival at the detector are measured. The entire spectrum can be cycled every 100 μsec. In essence, this technique allows the determination of the cell contents in real time. In a kinetic experiment, however, only one ion, produced upon ionization of either a reactant or product molecule, is monitored with time. The temperature range of our stop-flow system is 250K-450K. Second order recaction rate constants between 2×10^{-23} $cm^3 molecule^{-1} s^{-1}$ and 5×10^{-17} $cm^3 molecule^{-1} s^{-1}$ are amenable to accurate measurement within this system. Since this range of rate coefficients corresponds to that expected for many molecule-molecule reactions, this technique was proposed for the study of Reactions (1) and (2).

When stop-flow time-of-flight mass spectrometry experiments were performed on Reactions (1) and (2), it was found that within experimental error addition of one reactant to the reaction vessel had no effect on the rate of disappearance of the other reactant. We thus estimated that the rate constants for these processes are $\leq 1 \times 10^{-23}$ $cm^3 molecule^{-1} s^{-1}$.

Having found that the rate constants for Reactions (1) and (2) are too slow to be measured by the above technique, we devised a time-resolved infrared spectroscopy study of these reactions. An optical absorption cell seasoned with the haloborane prior to each experiment was filled with a few torr of the haloborane and 350-500 torr of oxygen. Haloborane infrared absorption intensities were then monitored as functions of time. Typical results of these experiments are plotted in Figure 2. The haloborane decay rates are seen to be extremely slow and, because wall loss effects may have been contributing to the observed decays, the rate constants extracted from these pseudo-first order decays must be considered as upper limits. Our knowledge of these rate constants thus remains limited to the expressions $k_1 \leq 1 \times 10^{-30}$ $cm^3 molecule^{-1} s^{-1}$ and $k_2 \leq 4 \times 10^{-25}$ $cm^3 molecule^{-1} s^{-1}$.

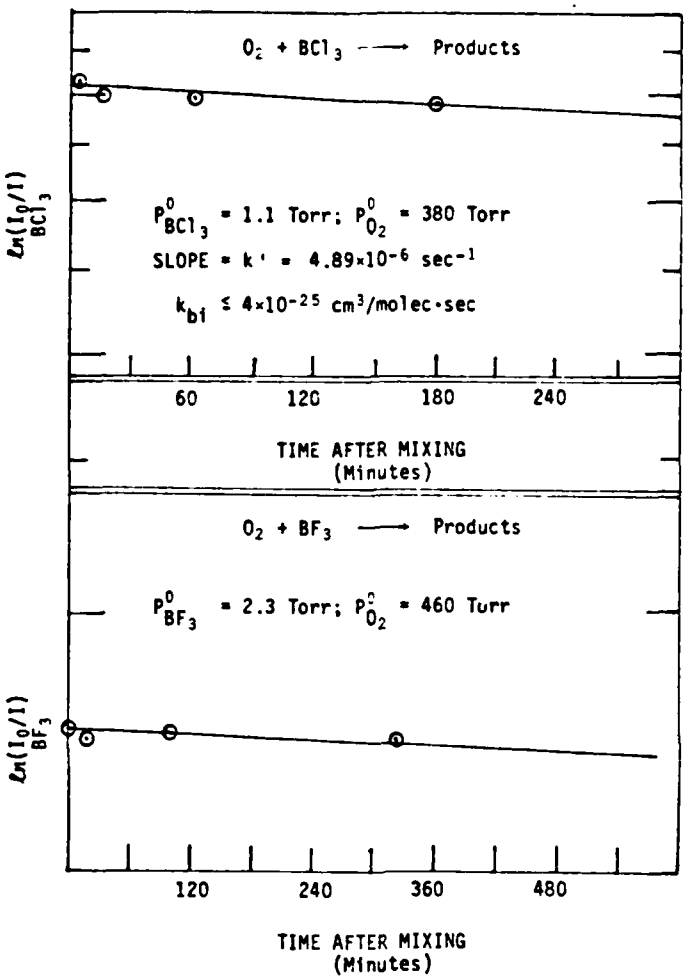

Figure 2. Time-Resolved Infrared Spectroscopy.

Having observed nearly negligible reactivities for the reactions O_2 + BF_3/BCl_3, we decided to probe the general oxidative behaivor of the haloboranes in more detail by studying their reactions with more active oxidizing agents. Investigations of the following reaction processes were made:

$$O_3 + BF_3 \rightarrow \text{Products} \quad (3)$$

$$O_3 + BCl_3 \rightarrow \text{Products} \quad (4)$$

$$H_2O + BCl_3 \rightarrow \text{Products} \; . \quad (5)$$

Again using the technique of time-resolved infrared spectroscopy, Reaction (3) was investigated and found to be immeasurably slow at room temperature. This reaction, then, was not looked at further. The study of Reaction (4), on the other hand, proved to be very interesting. Time-sequenced sets of complete infrared spectra of reacting $O_3/BCl_3/Ar$ mixtures were taken. The initial BCl_3 and argon pressures were measured using a capacitance manometer and the initial O_3 pressure was calculated from UV absorption measurements made at 254 nm. The initial reactant partial pressures were varied by as much as factors of four in different runs. The BCl_3 and O_3 decay rates and reaction product buildup rate (as shown in Figure 3a, a reaction product peak not observed in the pure O_3 or pure BCl_3 spectra grows with time) are calculated from the peak intensities in the sequential infrared spectra. Relative concentration vs. time after mixing plots for a typical experimental run are displayed in Figure 3b. It is seen that the rate of growth of the reaction product closely images the rate of decay of the BCl_3 reactant. It is worth noting here, however, that the bimolecular rate constants calculated from such plots do show a slight tendency to increase with increasing $[O_3]_{t=0}/BCl_3]_{t=0}$ ratios. These variations are likely due to the overall stoichiometry of the reaction.

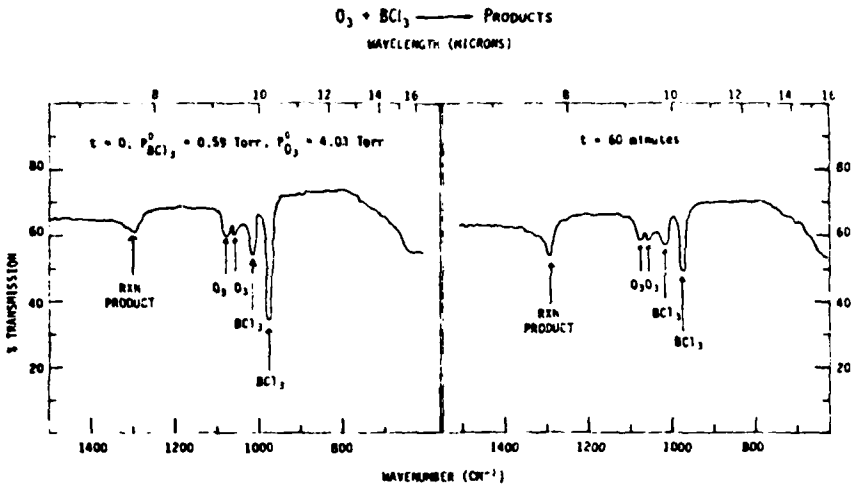

Figure 3a. Time-Resolved Infrared Spectroscopy of O_3-BCl_3 System.

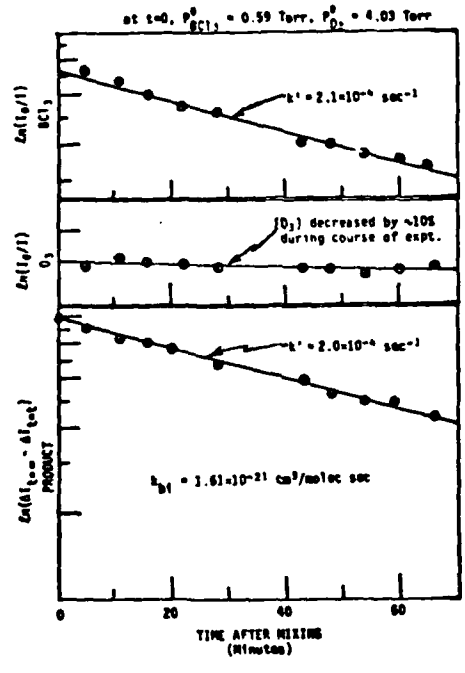

Figure 3b. First Order Decay Plot for the Disappearance of BCl_3 and Appearance of Reaction Product in the Reaction Product in the Reaction of BCl_3 with O_3 · $[O_3] > [BCl_3]$.

Three other experimental techniques were applied to the study of Reaction (4): (1) time-resolved UV absorption spectroscopy, (2) stop-flow time-of-flight mass spectrometry, and (3) reaction end product analysis. The results of these studies will be discussed below in turn.

A schematic of the simple but very powerful technique of time-resolved UV absorption spectroscopy is given in Figure 4a. Light from a mercury lamp at 253.7 nm was passed through an absorption cell containing the O_3BCl_3/Ar mixture. The transmitted intensity was monitored as a function of time by a filtered photodiode. Experiments were run with $[BCl_3]$ in varying excesses over $[O_3]$, ozone being the monitored species. Use of this technique required considerable caution. Since 253.7 nm radiation is absorbed by ozone via the photodissociative reaction $O_3 \xrightarrow{h\nu} O(^1D) + O_2$, the possibility existed that the atomic oxygen formed in the probe process could contribute to the chemistry under study. By using a variety of ozone concentrations and 253.7 nm radiation fluxes, however, it was conclusively shown that such probe-induced processes were unimportant. Furthermore, by allowing the low concentration reactant ozone to undergo complete reaction and the measuring essentially no absorption of 253.7 nm radiation, it was clearly demonstrated that the products of the reaction were not absorbing the probe radiation and thereby biasing the kinetic results. Thus the time variation of the transmitted 253.7 nm intensity generates an accurate time history of the ozone concentration. The experiments were run under pseudo-first order conditions with BCl_3 in excess and, as shown in Figure 4b, the bimolecular rate constant was obtained as the slope of a plot of the pseudo-first order decay constant vs. the BCl_3 concentration. A value of k_{bi} (298K) = 8.31×10^{-21} $cm^3 molecule^{-1} s^{-1}$ was obtained.

Reaction (4) was also studied by the previously described technique of stop-flow time-of-flight mass spectrometry. Small concentrations of BCl_3

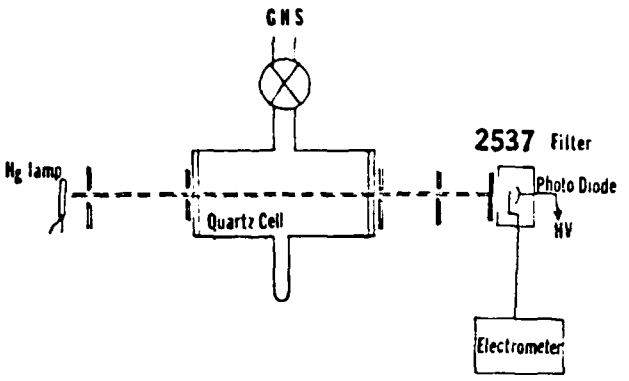

Figure 4a. Time-Resolved UV Absorption in O_3 + BCl_3 Reaction.

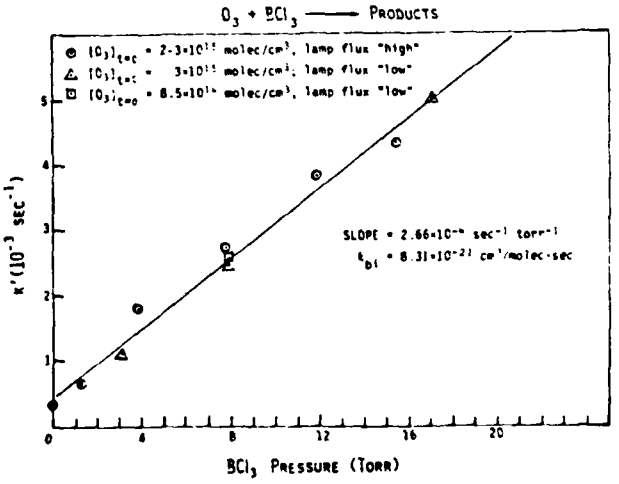

Figure 4b. Plot of O_3 Decay Rate vs. $[BCl_3]$.

in varying excesses of ozone were mixed in the reaction vessel and the time variation of the BCl_2^+ ion was followed mass spectrometrically. Typical decay curves are shown in Figure 5a; a bimolecular rate constant of $k_{bi} = 1.2 \times 10^{-20}$ $cm^3 molecule^{-1} s^{-1}$ was calculated by the usual methods. Averaging this result with that obtained using time-resolved UV absorption spectroscopy techniques, one obtains a room temperature rate constant for Reaction (4) of $k_{bi} = (1.0 \pm 0.3) \times 10^{-20}$ $cm^3 molecule^{-1} s^{-1}$. It is worth noting here that this value exceeds that obtained in the time-resolved infrared spectroscopy experiments (see Figure 3) by about a factor of six. Though we do not feel that we can adequately explain this discrepancy, it is probable that it is at least in part related to wall absorption of ozone in the extended duration infrared spectroscopy experiments.

Mass spectrometric studies of Reaction (4) were also performed by time sequenced sweeps of the entire mass spectrum. From top to bottom, Figure 4b shows respectively the mass spectrum obtained for pure ozone, that obtained for pure BCl_3, and that obtained a substantial period of time after mixing a small concentration of BCl_3 with a large excess of ozone. Close examination reveals that the observed product patterns differ substantially from the superposition of the pure O_3 and pure BCl_3 traces. In Table I we have listed those significant mass peaks observed in the mixed O_3/BCl_3 system which were found to be of only minor importance in either pure spectrum. Species such as BO, BO_2, BClO, Cl_2 and HCl have been identified. Other significant mass peaks remain unassigned at this time.

Finally, an end product analysis investigation of Reaction (4) was undertaken. Ozone and BCl_3 were mixed in a reaction vessel and allowed to react to completion. The techniques of infrared and UV absorption spectroscopy and expansion of condensable and non-condensable gases into calibrated volumes were utilized in the product analysis. As can be seen in Table II,

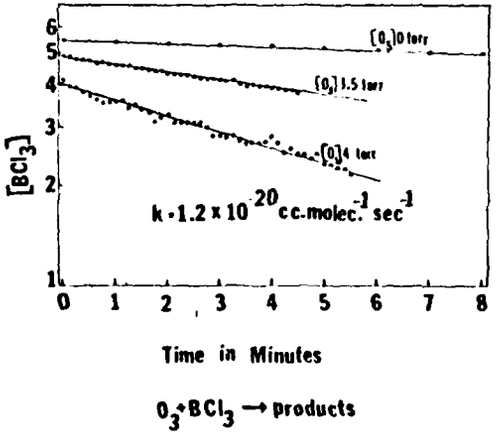

Figure 5a. Stop-Flow Time-if-Flight Study of $BCl_3 + O_3$ Reaction. Plots of First Order Decay of BCl_3 in Excess O_3.

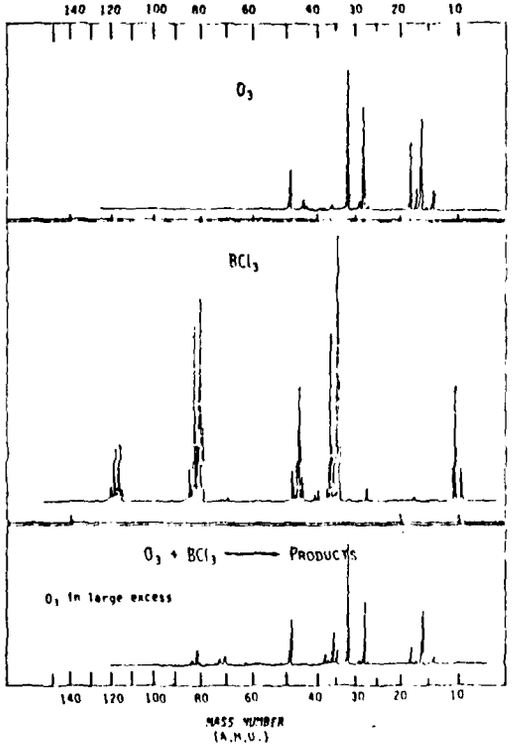

Figure 5b. Stop-Flow Time-of-Flight Study of $BCl_3 + O_3$ Reaction. Mass Spectra of Reactants and Products.

Table I.

SIGNIFICANT MASS SPECTRAL PEAKS ORSERVED IN THE O_3 + BCl_3 SYSTEM WHICH WERE FOUND TO BE OF ONLY MINOR IMPORTANCE IN THE MASS SPECTRA OF PURE O_3 AND/OR PURE BCl_3.

MASS NUMBER	POSSIBLE ASSIGNMENT
26	BO
27	BO
29	?
31	?
34	?
36	HCl
38	HCl
42	BO_2
43	BO_2
51 OR 52	?
57	?
62	BClO
63	BClO
64	BClO
70	Cl_2
72	Cl_2
77	?
110	?

Table II. End Product Analysis in O_3 + BCl_3 Reaction.

	RUN 1	RUN 2	RUN 3
$-BCl_3$	?	1.3×10^{19} MOLECULES	1.7×10^{19} MOLECULES
$-O_3$	2.3×10^{19} MOLECULES	1.8×10^{19} MOLECULES	2.0×10^{19} MOLECULES
$+Cl_2$	2.8×10^{19} MOLECULES	1.9×10^{19} MOLECULES	2.2×10^{19} MOLECULES
$+O_2$	1.5×10^{19} MOLECULES	1.3×10^{19} MOLECULES	1.3×10^{19} MOLECULES

$$2BCl_3 + 3O_3 \longrightarrow \begin{matrix} BO_2(?) \\ B_2O_3(?) + 3Cl_2 + 2O_2 \\ B_2O_5(?) \end{matrix}$$

the loss of BCl_3 molecules was found to be about 2/3 that of the gain in Cl_2 molecules: chlorine balance seems assured through the formation of Cl_2. Since the number of condensable boron oxide molecules formed could not be measured, the boron and oxygen balances cannot be definitively assigned. One notices, however, that the loss of ozone molecules exceeds the loss of BCl_3 molecules, possibly by as much as a 3:2 ratio. If such stoichiometry is assumed, then the overall Reaction (4) mechanism could be represented by reaction expressions of the type (or linear combinations thereof) listed at the bottom of Table II.

An abbreviated stop-flow time-of-flight mass spectrometry study was also performed on Reaction (5). This reaction was found to be fast, probably heterogeneous, and produced HCl and condensable boron oxides in high yield. Indeed, the addition of pure BCl_3 to a reaction vessel which had previously contained H_2O resulted in both the fast decay of BCl_3 and the obvious formation of HCl. In experiments in which BCl_3 and H_2O were mixed in the gas phase, the molecular leak of the reaction vessel very quickly became clogged resulting in the termination of gas flow into the mass spectrometer analyzer.

The above described studies of Reactions (1) through (5) have resulted in some interesting information concerning the general oxidative behavior of the haloboranes. Equally important, they have provided sufficient knowledge to make possible studies of more plume-relevant processes such as the radical-molecule reaction

$$O(^3P) + BF_3/BCl_3 \rightarrow \text{Products} .$$

III. KINETIC STUDY OF THE REACTION OF OH WITH H_2 AND D_2 FROM 250 to 1050 K

INTRODUCTION

The high temperature kinetic data needed for combustion modeling has been mainly derived from shock tube and flame studies. In these experiments, the accuracy of the obtained rate data is dependent on the degree of understanding of the chemistry involved in the system that is studied. In many cases it has been found that the extrapolation of the derived high temperature (T > 1000K) data to low temperatures (T > 500K) yield rate coefficients which disagree with the results of direct low temperature measurements. It has recently been recognized that this discrepancy could be due to either non-Arrhenius behavior[1,2,3] of the reaction under study or to systematic errors in the high temperature data. To fully understand the variation of the rate coefficients with temperature in the intermediate temperature range, i.e., 298 > T > 1000K, direct experimental measurements of elementary reaction rate coefficients are needed. This need has recently encouraged adaptation of proven low temperature kinetic technique to intermediate and high temperature studies. The developments have provided techniques which can directly measure the rate coefficient for an elementary reaction over a wide temperature range, thus minimizing the chances of relative systematic errors.

In parallel to these experimental developments, great strides have been made in theoretical calculations of elementary reaction rate coefficients.[4,5] The transition state theory has evolved to a point where quite rigorous calculations of thermal rate coefficients can be carried out. This ability can be largely attributed to the availability of calculated (ab initio) potential energy surfaces for many atom-diatom reactions and even four atom reactions such as $OH + H_2$.[6]

We have recently adapted the conventional technique of flash photolysis-resonance fluorescence to measure OH reaction rate coefficients at temperatures

above 1000K.[7,8] The rate coefficient for the reaction,

$$OH + H_2 \xrightarrow{k_1} H_2O + H \qquad (1)$$

was measured in the temperature range of 298-992K and the ℓnk_1 vs. 1/T plot was found to be non-linear.[7] Since our measurement of k_1, an ab initio calculation of the potential energy surface for this reaction,[6] as well as a transition state theory calculation[5] of k_1 which utilized this surface, have been reported. The potential energy surface for the OH + H_2 reaction would be nearly identical to that of OH with D_2,

$$OH + D_2 \rightarrow DHO + D \qquad (2)$$

and therefore comparison of measured values of k_2 with those calculated would constitute a direct test of the theory. Also, the question of how isotopic substitution affects the curvature of Arrhenius plots is worth investigating. Therefore, with the hope of testing the theory and furthering our understanding of this elementary reaction, we have measured k_2 over the temperature range of 250-1050 K.

Even though both k_1 and k_2 have been measured by many investigators, they have not been studied using one direct technique which can cover a wide temperature range. As mentioned earlier, we have measured k_1 in the temperature range of $298 < T < 992$ K. However, to obtain a consistent set of data for k_1 and also since k_1 has been measured only by one group at $T < 298$K,[9] we extended the measurement of k_1 to 250K.

The technique of flash photolysis-resonance fluorescence as adapted for high temperature studies was utilized in carrying out all the reported measurements. A detailed description of this technique is given in this paper.

EXPERIMENTAL SECTION

The utilization of flash photolysis-resonance fluorescence (FP-RF) technique in studies of OH radical reactions at temperatures below 500K are amply described in the literature.[10,11] We have recently adapted this technique for studies at temperatures up to ∿ 1200K. In this paper we will describe our high temperature system in detail.

The primary difficulty in using the FP-RF technique at high temperatures is maintaining good OH detection sensitivity while using a reactor which can be operated at these temperatures. We spent a considerable amount of time experimenting with various cell designs, cell materials, focusing optics, and light baffle arrangements to maximize OH detection sensitivity and still be able to heat the reactor to high temperatures. The final apparatus configuration that was adopted is shown in Figure 1. The principal system components are (1) a thermostated reaction cell, (2) a spark discharge flash-lamp perpendicular to one face of the cell, (3) a CW OH resonance lamp perpendicular to the photolysis beam, (4) a bandpass filter/photomultiplier combination for monitoring OH resonance fluorescence emitted perpendicular to both the photolysis and resonance radiation beams, and (5) a signal averager and fast photon counting electronics.

The reactor was built out of quartz. Five highly polished Suprasil windows were fused to the cell using quartz tape. This cell was coated with graphite on the outer surface. Once baked, the graphite bonded well with the quartz surface. This black graphite coating served two purposes: (1) it cut down the amount of scattered radiation, and (2) it formed a good thermally conductive surface which helped avoid 'hot spots'. This cell was heated using tantalum wire windings which were contained inside ceramic tubes. The heaters were powered by a constant voltage power supply. The temperature

could be controlled by changing the applied voltage using variacs. The cell and the insulated heaters were covered with at least 5 layers of thin stainless steel sheets which acted as radiation shields, thereby minimizing the heat loss from the cell. A chromel-alumel thermocouple was attached to the outer surface of the reactor primarily to aid in knowing the temperature of the cell during heating and cooling periods. The temperature of the gas inside the reactor was directly measured using a thermocouple which was inserted into the reactor. In preliminary characterization experiments the temperature differential between the upper and lower portions of the reaction zone (maximum length $\sim$ 2 cm) was found to be < 5K at 1000K and unmeasurable at 500K. The bottom window (fluorescence port located $\sim$ 5 cm below the active volume) was measured to be $\sim$ 15K below that of the active volume at 1000K when the gases were flowing through the cell. Therefore, it can be quite confidently ascertained that at 1000K the temperature in the active zone was constant to within 5K and known to better than 10K.

Quartz (unlike pyrex) transmits 310 nm radiation and thus increases the background scattered resonance lamp radiation that reaches the detector. To overcome this problem, two modifications were carried out. (a) The microwave discharge lamp, the source of resonance radiation, was moved away ($\sim$ 80 cm) from the cell. A 5 cm diameter quartz convex lens was placed $\sim$ 20 cm from the discharge to collect the radiation and render it nearly parallel. A second 5 cm diameter quartz lens located $\sim$ 15 cm from the center of the reactor, focused this parallel beam on the far port of the reactor. This configuration enabled almost all reasonance radiation to pass only through the cell windows. (b) The photon counting electronics were improved to count linearly up to 3 MHz. With this combination, the measured background count rate ranged from 100-200 KHz. (It should be pointed out that generally emphasis is placed on reducing the background rate to a very low value, often

at the expense of decreasing the amount of resonance radiation that enters the reactor.) The output of the N_2 flashlamp was collimated by a set of baffles and then rendered parallel by a pith polished Suprasil lens which ensured that all flash radiation exited only through the windows. In addition, a set of lenses was employed to collect the OH fluorescence from the center of the cell and then focus it onto the photocathode of a RCA 8850 photomultiplier tube. Use of this lens set resulted in increases in both fluorescence signal and background light with a large improvement in signal-to-noise ratio.

To determine the sensitivity of the apparatus, we carried out back-to-back experiments at 298K where the signal/noise per flash was determined under typical experimental conditions (flash energy = 70J, 50 mTorr H_2O, 100 Torr Ar) and compared with the signal/noise per flash obtained under conditions where a known OH concentration could be produced. (Here, the signal/noise is defined as the ratio of signal due to OH to the square root of the background counts.) The procedure used to generate a known concentration of OH involved replacing the flashlamp with a frequency quadrupled pulsed 266 nm laser beam (from a Nd:YAG laser) and adding $\sim$ 5 mTorr O_3 to the reaction mixture. Upon photolysis the following reactions take place:

$$O_3 \xrightarrow[266\ nm]{h\nu} \begin{cases} O(^1D) + O_2(^1\Delta_g) \\ O(^3P) + O_2(^3\Sigma) \end{cases}$$

$$O(^1D) + Ar \rightarrow O(^3P) + Ar$$

$$O(^1D) + H_2O \rightarrow 2\ OH \quad .$$

The laser beam was expanded so its cross-sectional area as it traversed the reaction cell was approximately equal to that of the flashlamp radiation. The laser power was measured at the rear of the cell with an absolute energy

monitor and corrected for the loss due to reflection by the back window (~ 10%). Since the absorption cross section for O_3 at 266 nm,[12] the quantum yield for $O(^1D)$ from O_3 at 266 nm (~ 0.9),[13] the rate coefficients for $O(^1D)$ quenching by Ar[14] and reaction with H_2O[15] are known, we could determine the concentration of OH in the reactor.

The results of actinometry indicate that, for the reaction mixture employed, ~ 1×10^9 OH per cm^3 could be detected (signal/noise = 1) with an integration time of 1×10^{-3}s. Extrapolation of this result to other experimental conditions shows that all experiments were carried out with OH concentrations between 1×10^{10} and 1×10^{11} per cm^3. It was also found that as long as the reactor was kept clean, the measured signal for a given OH concentration did not deteriorate significantly with increases in temperature.

All experiments were carried out under pseuto-first order kinetic conditions with $[H_2]$ and $[D_2]$ in large excess over [OH]. ($[H_2]/[OH]$ and $[D_2]/[OH]$ ratios were always greater than 1000. $[H_2]$ ranged from ~ 2×10^{13} to 2×10^{17} cm^{-3} and $[D_2]$ ranged from ~ 2×10^{13} to 1×10^{18} cm^{-3}.) OH radicals were produced by flash photolysis of H_2O at wavelengths between the Suprasil cutoff at 165 nm and the onset of continuum absorption at 185 nm (flash duration ≤ 50 μsec). Following the flash, weakly focused OH resonance lamp radiation continuously excited a small fraction of the OH in the reactor to the electronically excited $A^2\Sigma^+$ state; the resultant (0,0) band A → X fluorescence emanating in the direction perpendicular to both the resonance excitation and photolysis beams was collected by a lens and focused onto a photomultiplier fitted with a bandpass filter (309.5 nm peak transmission, 10 nm FWHM). Signals were obtained by photon counting and then fed into a signal averager operated in the multichannel scaling mode. For each decay rate measured, sufficient

flashes (50-1000) were averaged to construct a well-defined temporal profile over at least a factor of twenty variation in [OH].

All experiments were carried out under "slow flow" conditions. The flow rate through the reactor was such that each photolysis flash encountered a fresh reaction mixture (photolysis repetition rate $\sim$ 0.3 Hz). At temperatures greater than 270K, $H_2(D_2)$ was flowed from a 12ℓ source bulb containing $H_2(D_2)$/diluent gas at 800 Torr through distilled water at room temperature. The $H_2(D_2)$ diluent gas mixture, H_2O/diluent gas mixture, and additional diluent gas were mixed prior to entering the reaction cell. Concentration of each component in the reaction mixture was determined from measurements of the appropriate mass flow rates (measured using calibrated mass flow meters) and the total pressure. At temperatures below 270K, the amounts of H_2 and D_2 needed to carry out the experiments were so large that pure H_2 or D_2 was needed in the source bulb. Therefore, we prepared large amounts of $H_2(D_2)$/diluent mixtures in an $\sim$ 40ℓ volume and flowed it directly into the reactor after mixing it with a small amount of H_2O/diluent mixture. This procedure avoided any possible flow meter calibration errors.

The gases used in this study had the following stated purities: Ar > 99.9995%, H_2 > 99.9999%, D_2 > 99.96%. Also, the D_2 mixture had less than 1 ppm of organics (mainly as CH_4) and an isotopic purity of 99.5%. H_2 and D_2 were passed through liquid nitrogen traps filled with glass beads before being used to remove any condensible organics. Ar was used as supplied.

RESULTS

All experiments were carried out under pseudo-first order conditions with $[H_2]$ or $[D_2]$ >> [OH]. The temporal profile of [OH], then, is given by the equation,

$$\ell n\{[OH]_o/[OH]_t\} = (k_x[x] + k_d)t = k't$$

where X is either H_2 or D_2, k_d is the first order rate constant for the loss of OH in the absence of X, and k' is the measured pseudo-first order rate constant. [OH] decays were observed to be exponential for at least three 1/e times as typified by data shown in Figure 2; the exponential [OH] decay validates the existence of first order conditions. At each temperature, the [OH] decay rates were measured at several (minimum 4, on the average 6) fixed reactant concentrations. The bimolecular reaction rate constant was obtained from the slope of the k' vs. reactant concentration plots. Figure 3 shows one such plot for k_2 at 932K. The measured values of k_1 and k_2 at various temperatures are listed in Tables I and II, respectively. The quoted errors are 2σ and represent the precision of the measured rate coefficient. It is estimated that the accuracy at 298K is $\sim$ 12% decreasing to $\sim$ 20% as the temperature is either raised to 1000K or lowered to 250K.

It has been previously shown that under our experimental conditions radical-radical reactions such as H + OH or OH + OH are insignificant.[11] To ensure that our present results were devoid of such secondary reactions the $[OH]_o$, the flash energy, the $[H_2O]$, and the system pressure, were varied at most temperatures. The results indicated the absence of any secondary reactions contributing to the measured value of k_1 and k_2.

The values of k_1 and k_2 are quite small at low temperatures. Therefore, very small concentrations of reactive impurities, in the order of 10^{-4}%, can contribute significantly to the measured values if they are present. It is always very hard to completely rule out this possibility of impurity reactions. Our samples of H_2 and D_2 are very pure. Both H_2 and D_2 have less than 1 ppm of CH_4, the only organic that was present in measurable quantities. Great care was taken to ensure that no impurities were added in the course of transferring H_2 and D_2 from the tanks to the reactor. Therefore we believe that our values of k_1 and k_2 are accurate to at least 20% at 250K.

Figure 4 shows plots of ℓnk_1 and ℓnk_2 vs. 1/T. Results of our previous measurements of k_1 in the temperature range of 298 to 1000 K are also included. It is clear that Arrhenius plots are not linear for both k_1 and k_2; ℓnk_2 vs. 1/T being more nearly linear than ℓnk_1 vs. 1/T. We previously fit k_1 values between 298K-1000K to the function $k(T) = 4.12 \times 10^{-19} T^{2.44} \exp(-1281/T)$ while Zellner[2] obtained $k(T) = 1.66 \times 10^{-16} T^{1.6} \exp(-1660/T)$ based on all previous measurements. Our present data is best described by the former of the two expressions. A similar three-parameter expression for Reaction (2) based solely on our data is, $k_2(T) = 4.37 \times 10^{-15} T^{1.18} \exp(-2332/T)$.

DISCUSSION

Reaction (1) has been studied by numerous investigators[16,17,18,19] at room temperature. There are four studies of k_1 as a function of temperature.[9,20,21,22] With the exception of Westenberg and deHaas,[21] all previous studies had an upper temperature limit of 500K. Table III lists both the 298K value and, where appropriate, the Arrhenius parameters. There is reasonable agreement between various k_1 (298K) values. As pointed out earlier the $\ell n k_1$ vs. 1/T (Arrhenius) plot is not linear. For the sake of comparison we have fitted our low temperature (T < 400K) data to an Arrhenius expression which yields;

$$k(T) = (4.9 \pm 0.5) \times 10^{-12} \exp[(1.99 \pm 0.34) \times 10^3/T] \text{ cm}^3\text{molecule}^{-1}\text{s}^{-1}$$

where the errors are 2σ and $\sigma_A = A\, \ell_{nA}$. These values are listed in Table III. Our value of A and E/R are in good agreement with other measurements except with Smith and Zellner's values. Smith and Zellner[9] were the only investigators who have measured k_1 at T < 298K. They encountered some difficulty at temperatures below 270K where they had secondary reactions such as

$$OH + OH + M \rightarrow H_2O_2 + M \qquad (6)$$

and

$$OH + H + M \rightarrow H_2O + M \; . \qquad (7)$$

Contributing to the measured OH temporal profile. They corrected their measured value to take into consideration the contributions of these secondary reactions. The value of $2k_6 + k_7$ they used to correct their data was $\sim 7 \times 10^{-30}$ $\text{cm}^6\text{molecule}^{-2}\text{s}^{-1}$ which in the light of recent measurements[23] seems rather high. Therefore it can be postulated that they over corrected their low temperature value which could account for the larger E/R values. Figure 4 shows the Arrhenius plots reported by Greiner,[20]

Smith and Zellner,[9] and Atkinson et al.[22] It is clear from Figure 4 that our individual data points at T ≤ 298K are in excellent agreement with the line of Smith and Zellner. It is, however, our data T > 298K which are lower than that of Smith and Zellner's line. Therefore it is doubtful that the low temperature corrections of Smith and Zellner could account for the discrepancy. Also, at T > 298K, the results of Westenberg and deHaas, Atkinson et al., and Greiner are all in good agreement with our values of k_1. It is particularly interesting to note the agreement over the entire temperature range of our results with that of Westenberg and deHaas who were the first to notice the non-linear variation of $\ell n k_1$ with 1/T.

Reaction (2) has been measured by three separate groups all at 298K.[18,24,25] The temperature dependence of k_2 has been studied only by Smith and Zellner.[9] Table IV lists all available data on Reaction (2). Again for the sake of comparison, we have fit our low temperature data to an Arrhenius form and obtained A and E/R which are shown in Table IV. There is reasonable agreement between all measured values of k_2 (298K); our value being the lowest. Even the Arrhenius parameters derived in this study based on low temperature (i.e. T < 470K) data, $k_2(T) = (1.21 \pm 0.52) \times 10^{-12} \exp[(-2.67 \pm .15) \times 10^3/T]$ $cm^3 molecu\ e^{-1} s^{-1}$ agree well with that of Smith and Zellner.[9]

One of the main aims of this work was to obtain a set of data using a single technique over a wide temperature range for a set of related reactions such that a coherent data base will be available to compare present day theory with experimental results. Based on our data two observations can be made. (a) The $\ell n k$ vs. 1/T plots are not linear for both Reactions (1) and (2). (b) The kinetic isotopic effect, i.e., k_1/k_2 increases with decreases in temperature. Comparison of experimental results with theory can be made at different levels of quantification. The general non-linear Arrhenius behavior for reactions such as Reactions (1) and (2) can be qualitatively explained, and is even to be

expected, based on chemical kinetic theories of elementary reactions. Zellner[2] and Gardiner[3] have discussed the probable causes for this behavior which can be understood to different levels of precision based on the transition state theory and/or the collision theory.

Before comparing the theoretical calculations with experimental results, the mechanism for the reaction of OH with hydrogen needs to be explicitly stated. This reaction seems to proceed through the bond scission in hydrogen,

$$H_aO + H_b - H_b \rightarrow H_aOH_b + H_b$$

rather than the O-H bond cleavage

$$H_aO + H_b - H_b \rightarrow H_b - O - H_b + H_a \ .$$

This assumption is made in all calculations and is seldom stated explicitly. There is evidence to justify this mechanism based on the work of Westenberg and deHaas[21] who observed the almost exclusive production of H atoms in the reaction of OD with H_2 (rather than D atoms which would be produced if the bond in hydroxyl radical was cleaved) and the work of Paraskevopoulos and Nip,[25] who noted the absence of kinetic isotopic effect between the reaction of OH with H_2 and OD with H_2.

The transition state theory can be used at many levels of rigor to calculate the value of $k_1(T)$ and $k_2(T)$ (and hence $K_1(T)/k_2(T)$). Assuming a transition state structure one can predict the temperature variation of the bimolecular rate coefficient k, especially when the transition state properties are made to fit the value of k measured at one temperature. Recently, however, ab initio potential energy surfaces have been calculated for simple atom-diatom reactions and even four atom reactions such as Reactions (1) and (2).[6] Using this potential energy surface, conventional transition state theory calculations have been carried out by Schatz and Walch[5] and Isaacson and Truhlar[26] for Reaction (1) and by Schatz and Wagner[27] and Isaacson and Truhlar[26] for Reaction (2). Isaacson and Truhlar[26] have also calculated $k_1(T)$ and $k_2(T)$ based on canonical

variation theory. Figures (5) and (6) show the calculated values of $k_1(T)$ and $k_2(T)$, respectively, based on conventional transition state theory which includes and excludes tunneling as well as the canonical variation theory which excludes tunneling. Two points are clear: (a) calculated $k_1(T)$ values are much lower than experimental values when tunneling is neglected, the discrepancy between calculated and experimental values increasing with decreasing temperature, and (b) the $k_2(T)$ values which are calculated on the same potential energy surface as that for Reaction (1) and which includes tunneling correction, predicts $k_2(T)$ values much lower than measured values.[27] The fact that the calculated rate coefficients are very sensitive to the exact choice of input parameters is seen when we compare the results of Schatz and Walch[5] with those of Isaacson and Truhlar.[26] Using the same potential energy surface, they obtain different results which are directly attributed to differences in partition functions, and the incorporation of anharmonicity, spin orbit coupling, etc. The canonical variation theory calculations which exclude tunneling yield the lowest calculated values for both $k_1(T)$ and $k_2(T)$. In fact, the difference between the calculated and measured values of $k_1(T)$ at 250K is $\sim$ a factor of 20. However, it is expected that inclusion of tunneling would greatly enhance the agreement between calculations and experimental results. It should be noted that all these calculations suggest that tunneling is a major contributor to the overall rate coefficient for the reaction and the tunneling contribution increases quite dramatically with decreases in temperature.

Another experimental parameter which can be compared with theoretical calculations is the kinetic isotope effect, i.e., k_1/k_2. Table V lists these values for all the cases considered above as well as the calculations of Smith and Zellner. Smith and Zellner[9] used two different semiempirical surfaces,

i.e., LEPS and BEBO, and they neglected tunneling. It should also be noted that they assumed the energy barrier height to be the same as the experimentally measured activation energy. It is clearly seen that all calculations show the observed trend in k_1/k_2, i.e., decrease with increase in temperature. Moreover, it is interesting to see that the best agreement between measured and calculated values of k_1/k_2 is obtained when tunneling is neglected. Even in the case of the semiempirical calculation of Smith and Zellner, there is good agreement between measured and calculated kinetic isotope effects. In fact, this surprising agreement led to the speculation that tunneling is probably not important in Reactions (1) and (2). However, in spite of the good agreement in isotope effect ratios, the absolute values of k_1 and k_2 are grossly underestimated when tunneling is neglected as shown by calculations of Schatz et al.[5,27] and Truhlar et al.[26]

At this point one is forced to ask the question, even if an accurate ab initio potential energy surface is available, can the present theories accurately predict thermal rate coefficients, and, can the theories shed more light on the exact nature of the reactive process. Based on the calculations that are presented it is seen that even though great strides have been made in this direction, the theory still needs to be refined to predict rate coefficients with the accuracy of 10-50%. Of course, it should always be kept in mind that ultimately the agreement between theory and experiment is a reflection on the accuracy of the potential energy surface itself.

The explanation of the non-Arrhenius behavior of k_1 and k_2 based on the collision theory has been discussed by Zellner[2] and Gardiner.[3] As pointed out by Zellner,[2] if the rate coefficient for the reaction of OH(v=1) with H_2 is $\sim$ 150 times that for H_2(v=0), then depending on the efficiency with which the increased vibrational energy can help hasten the reaction, the observed

thermal rate coefficient can exhibit different degrees of non-Arrhenius curvature. Zellner et al.[28] have observed that $H_2(v=1)$ is removed by OH with a rate coefficient of $\sim 1 \times 10^{-12}$ $cm^3 molecule^{-1} s^{-1}$. If this removal is attributed totally to reaction rather than vibrational relaxation, a possibility that is not experimentally proven, then $H_2(v=1)$ can contribute significantly to $k_1(T)$ even at temperatures as low as 800K. Of course, this mechanism does not preclude contribution due to tunneling at low temperatures. In the absence of any data on $D_2(v=1)$ it is hard to speculate if such a process can contribute to k_2. It should be noted that the population of D_2 in v=1 would be much higher than that of H_2 and if $D_2(v=1)$ reacts as fast as $H_2(v=1)$ is postulated to do, the contribution of $D_2(v=1)$ can be more than that of $D_2(v=0)$ at temperatures as low as 900K, and hence would be easier to measure.

Finally, it is worth inquiring what experimental work can be carried out to further check and aid in the development of the theories of elementary reactions. Two experiments are suggested, (a) extension of measurement of k_1 and k_2 to temperatures much lower than 250K where tunneling should dominate and temperatures higher than 1000K where energetics are less important and (b) measure rate coefficients for the reaction of OH with HD. Since the same potential energy surface that is used for H_2 and D_2 will be applicable, it will be interesting to see if the theory can predict the measured thermal rate coefficients for the reaction of OH with HD. Both these experiments will be underway shortly in our laboratory.

REFERENCES

1. F. Dryer, D. Naegeli, and I. Glassman, Combust. Flame, 17, 270 (1970).

2. R. Zellner, J. Phys. Chem. 83, 18 (1979).

3. W. C. Gardiner, Jr., Acc. Chem. Res. 10, 326 (1977).

4. D. M. Golden, J. Phys. Chem. 83, 109 (1979) and references therein.

5. G. C. Schatz and S. P. Walch, J. Chem. Phys. 72, 776 (1980).

6. S. P. Walch and T. H. Dunning, J. Chem. Phys. 72, 1303 (1980).

7. F. P. Tully and A. R. Ravishankara, J. Phys. Chem. 84, 3126 (1980).

8. F. P. Tully, A. R. Ravishankara, R. L. Thompson, J. M. Nicovich, R. C. Shah, N. M. Kreutter, and P. H. Wine, J. Phys. Chem., submitted.

9. I.W.M. Smith and R. Zellner, JCS Far. Trans. II, 70, 1045 (1974).

10(a). D. D. Davis, S. Fischer, R. Schiff, J. Chem. Phys. 59, 628 (1974).

(b). A. R. Ravishankara, P. H. Wine, and A. O. Langford, J. Chem. Phys. 70, 984 (1979).

(c). A. R. Ravishankara, G. Smith, R. T. Watson, and D. D. Davis, J. Phys. Chem. 81, 2220 (1977).

11. P. H. Wine, N. M. Kreutter, and A. R. Ravishankara, J. Phys. Chem. 83, 3191 (1979).

12. R. D. Hudson, "Critical Review of UV Photoabsorption Cross Sections for Molecules of Astrophysical and Aeronomic Interest," Reviews of Geophys. and Space Physics, 9, No. 2, 1971.

13(a). J. C. Brock and R. T. Watson, Chem. Phys. Lett. 71, 371 (1980).

(b). C. E. Fairchild, E. J. Stone, and G. M. Lawrence, J. Chem. Phys. 69, 3632 (1978).

(c) R. R. Sparks, L. R. Carlson, K. Shobatake, M. L. Kowalczyk, and Y. T. Lee, J. Chem. Phys. 72, 1401 (1980).

14(a). R. F. Heidner, III and D. Husain, Int. J. Chem. Kinet. VI, 77 (1974).

(b). J. A. Davidson, H. I. Schiff, T. J. Brown, G. E. Streit, C. J. Howard, J. Chem. Phys. 69, 1213 (1978).

15. P. H. Wine and A. R. Ravishankara, Chem. Phys. Letts., in press and and references therein.

16. F. Kaufman and F. P. delGreco, Disc. Faraday Soc. 33, 128 (1962).

17. G. Dixon-Lewis, W. E. Wilson, and A. A. Westenberg, J. Chem. Phys. 44, 2877 (1966).

18. F. Stuhl and H. Niki, J. Chem. Phys. 57, 3171 (1972).

19. R. Overend, G. Paraskevopoulos, and R. J. Cvetanovic, Can. J. Chem. 53, 3374 (1975).

20. N. R. Greiner, J. Chem. Phys. 51, 5049 (1969).

21. A. A. Westenberg, and N. deHaas, J. Chem. Phys. 58, 4061 (1973).

22. R. Atkinson, D. A. Hansen, and J. N. Pitts, Jr., J. Chem. Phys. 63, 1703 (1975).

23. R. D. Hudson and E. I. Reed, "The Stratosphere: Present and Future," NASA Reference Publication 1049, 1979.

24. N. R. Greiner, J. Chem. Phys. 48, 1413 (1968).

25. G. Paraskevopoulos and W. S. Nip, Can. J. Chem. 58, 2146 (1980).

26. A. Isaacson and D. G. Truhlar, private communications, (1980).

27. G. Schatz and A. Wagner, private communications, (1980).

28. R. Zellner, W. Steinert, and H. Gg. Wagner, as reported in Ref. 2.

Table I. Rate Coefficient vs. Temperature for Reaction 1: $OH+H_2 \rightarrow H_2O+H$

Temperature (K)	k_1, $cm^3 molecule^{-1} s^{-1}$
250	$(1.69 \pm 0.14) \times 10^{-15}$
265	$(2.67 \pm 0.37) \times 10^{-15}$
282	$(4.14 \pm 0.30) \times 10^{-15}$
295	$(5.64 \pm 0.60) \times 10^{-15}$
333	$(1.28 \pm 0.05) \times 10^{-14}$
356	$(1.83 \pm 0.08) \times 10^{-14}$
366	$(2.02 \pm 0.21) \times 10^{-14}$
396	$(3.32 \pm 0.11) \times 10^{-14}$
960	$(2.40 \pm 0.25) \times 10^{-12}$
1050	$(3.20 \pm 0.44) \times 10^{-12}$

Table II. Rate Coefficient vs. Temperature for Reaction 2: $OH+D_2 \rightarrow DHO+H$

Temperature (K)	k_2, $cm^3 molecule^{-1} s^{-1}$
250	$(3.16 \pm 0.25) \times 10^{-16}$
268	$(5.00 \pm 0.57) \times 10^{-16}$
298	$(1.83 \pm 0.12) \times 10^{-15}$
336	$(3.98 \pm 0.17) \times 10^{-15}$
356	$(6.03 \pm 0.36) \times 10^{-15}$
366	$(7.07 \pm 0.71) \times 10^{-15}$
380	$(1.07 \pm 0.05) \times 10^{-14}$
398	$(1.18 \pm 0.18) \times 10^{-14}$
438	$(3.07 \pm 0.23) \times 10^{-14}$
449	$(3.35 \pm 0.14) \times 10^{-14}$
471	$(4.81 \pm 0.37) \times 10^{-14}$
525	$(8.86 \pm 0.85) \times 10^{-14}$
572	$(1.74 \pm 0.06) \times 10^{-13}$
605	$(1.61 \pm 0.10) \times 10^{-13}$
617	$(2.31 \pm 0.04) \times 10^{-13}$
664	$(3.47 \pm 0.20) \times 10^{-13}$
752	$(4.82 \pm 0.21) \times 10^{-13}$
788	$(5.93 \pm 0.34) \times 10^{-13}$
820	$(7.8 \pm 1.1) \times 10^{-13}$
932	$(1.11 \pm 0.03) \times 10^{-12}$
960	$(1.28 \pm 0.11) \times 10^{-12}$
1050	$(1.61 \pm 0.45) \times 10^{-12}$

Table III. Summary of Rate Constant Data for Reaction 1; $OH+H_2 \rightarrow H_2O+H$

k_1 (298) x 10^{15}, cm^3 $molecule^{-1}s^{-1}$	A x 10^{+12}, cm^3 $molecule^{-1}s^{-1}$	E/R, K^{-1}	Temperature Range, K	Technique	Reference
7.1 ± 1.7	--	--	--	DF-RF	16
6.5 ± 0.35	--	--	--	DF-ESR	17
7.9	$6.76^{+1.76}_{-1.39}$	2030 ± 91	300-500	FP-RA	20
7.1 ± 1.1	--	--	--	FP-RF	18
7.6	a	a	298-745	DF-ESR	21
7.1 ± 1.0	18^{+9}_{-6}	2330 ± 121	240-460	FP-RA	9
5.8 ± 0.3	--	--	--	FP-RA	19
6.97 ± 0.70	5.9	2009 ± 151	298-424	FP-RF	22
6.08 ± 0.37	4.9 ± 0.5	1990 ± 340	250-396	FP-RF	This work[b]

FP-RA; Flash photolysis-resonance fluorescence

DF-ESR; Discharge flow - ESR detection

FP-RF; Flash photolysis - resonance fluorescence

DF-RF; Discharge flow - resonance fluorescence

a: Observed curved ℓnk vs. 1/T plots, and hence did not report E/R values.

b: This expression has been derived from only the low temperature data.

Table IV. Summary of Rate Constant Data for Reaction 2.

k_2 (298) x 10^{15}, cm^3 $molecule^{-1}s^{-1}$	A x 10^{12} cm^3 $molecule^{-1}s^{-1}$	E/R k^{-1}	Temperature Range K	Technique	Reference
2.1 (± 12.5%)	--	--	--	FP-RA	24
2.05 ± 0.31	--	--	--	FP-RF	18
2.2 ± 0.4	$1.25^{+0.6}_{-0.4}$	2598 ± 182	210-460	FP-RA	9
2.11 ± 0.18	--	--	--	FP-RA	25
1.83 ± 0.12	1.21 0.52	2671 ± 147	250-470	FD-RF	This work

FP-RA; Flash photolysis - resonance absorption

FP-RF; flash photolysis - resonance fluorescence

Table V. Comparison of Experimentally Measured Kinetic Isotope Effect $(k_1(T)/k_2(T))$ with Calculated Values.

Temperature (K)	Experimental[a] Result	Smith & Zellner Ref(9)		Schatz, Walch, & Wagner, (Ref(5,27)	Isaacson & Truhlar Ref(26)		
		BEBO	LEPS	≠/W	≠	≠/W	CVT
250	5.4 ± 1.5			8.9	3.6	5.6	2.2
298	3.3 ± 0.9	3.6	3.7	7.0	3.3	4.9	2.2
400	2.5 ± 0.7[b]			4.3	2.9	3.9	2.1
600	1.7 ± 0.5[b]			3.3	2.3	2.8	2.0
1000	1.6 ± 0.5[b]			2.3	1.8	2.0	1.7

a: The quoted errors are ∿ 30% which is calculated based on the estimated accuracy of $k_1(T)$ and $k_2(T)$.

b: Since both $k_1(T)$ and $k_2(T)$ were not measured at exactly these temperatures. The three three parameter equation given in the text was used to calculate $k_1(T)$ and $k_2(T)$.

≠: Transition state theory using the potential energy surface calculated by Walch and Dunning (Ref. 6)

≠/W: Transition state theory using Wagner tunneling correction using the potential energy surface. Calculated by Walch and Dunning (Ref. 6).

CVT: Canonical variation theory using the potential energy surface calculated by Walch and Dunning (Ref. 6).

Figure Captions

1. Schematic diagram of the high temperature flash photolysis-resonance fluorescence apparatus. AD. amplifier discriminator; D, diluent gas; DVM, digital voltmeter; F1, 309.5 nm bandpass filter; FL flashlamp; FT, flow transduder; HC, high voltage capacitor; MC, mixing chamber; MCA, multichannel analyzer; MG, microwave generator; NV, needle valve; PG, pressure gauge; PM1, photomultiplier RCA 8850; PS, high voltage power supply; R/D, reactant/diluent gas; RL resonance lamp; TC, thermocouple; TTY, teletype; VM, vacuum housing.

2. Typical [OH] temporal profile following flash photolysis of $H_2O/D_2/Ar$ mixture. Experiental conditions: T = 932K; P = 100 Torr (Ar); Flash Energy = 80J; $[H_2O]$ = 70 mTorr; Concentration of D_2 in molecules cm^{-3}, (a) 1.08×10^{14}, (b) 2.09×10^{14}, (c) 4.88×10^{14}.

3. Plot of the pseudo-first order rate constant vs. $[D_2]$ at 932K. Solid line was obtained by linear least squares analysis of k' vs. $[D_2]$ date. Flash energy, o - 80J, □ - 200J.

4. Plots of ℓnk_1 and ℓnk_2 vs. 1000/T. For the sake of clarity, individual error bounds are not shown. o - k_1 values from Ref (7); □ - k_1 values from Ref (21), Arrhenius parameters reported by previous investigators are as follows: -·-, Smith and Zellner Ref (9); --- Atkinson et al. Ref (22); —— Greiner Ref (20).

5. Comparison of experimental values of $k_1(T)$ with calculations carried out using the ab initio surface of Dunning et al. Ref (6). —— TST calculation including tunneling correction (Schatz and Walch Ref. 5); --- TST calculation excluding tunneling (Schatz and Walch Ref. 5); —x— TST calculation including tunneling correction (Isaacson and Truhlar Ref. 26); —·— TST calculation excluding tunneling (Isaacson and Truhlar Ref. 26); —c— Canonical variation theory calculation excluding tunneling (Isaacson and Truhlar Ref. 26).

6. Comparison of experimental values of $k_2(T)$ with calculations carried out using the ab initio surface of Dunning et al. Ref (6). —— TST calculation including tunneling correction (Schatz and Wagner Ref. 27); —x— TST calculation including tunneling correction (Isaacson and Truhlar Ref. 26); —·— TST calculation excluding tunneling (Isaacson and Truhlar Ref. 26); —c— Canonical variation theory calculation excluding tunneling (Isaacson and Truhlar Ref. 26).

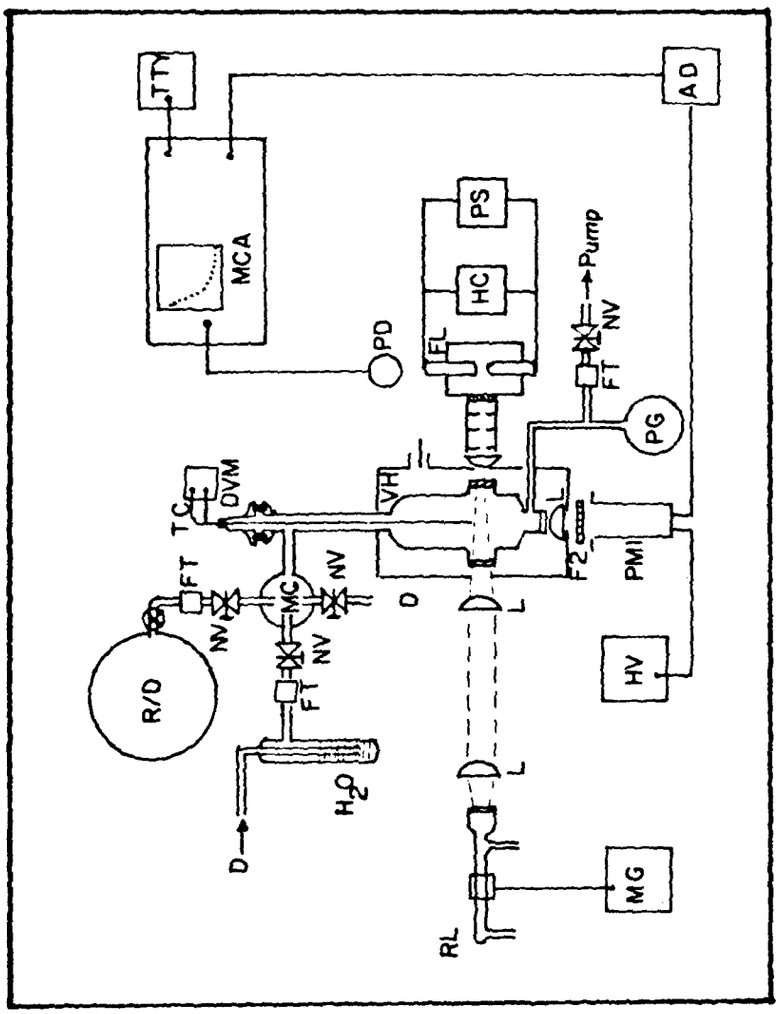
TT
AD
MCA
PS
HC
Pump
NV
FT
PD
EL
PG
VH
DVM
TC
L
F2
PMI
FT
NV
MC
NV
NV
D
L
R/D
NV
FT
HV
H_2O
D
L
MG
RL

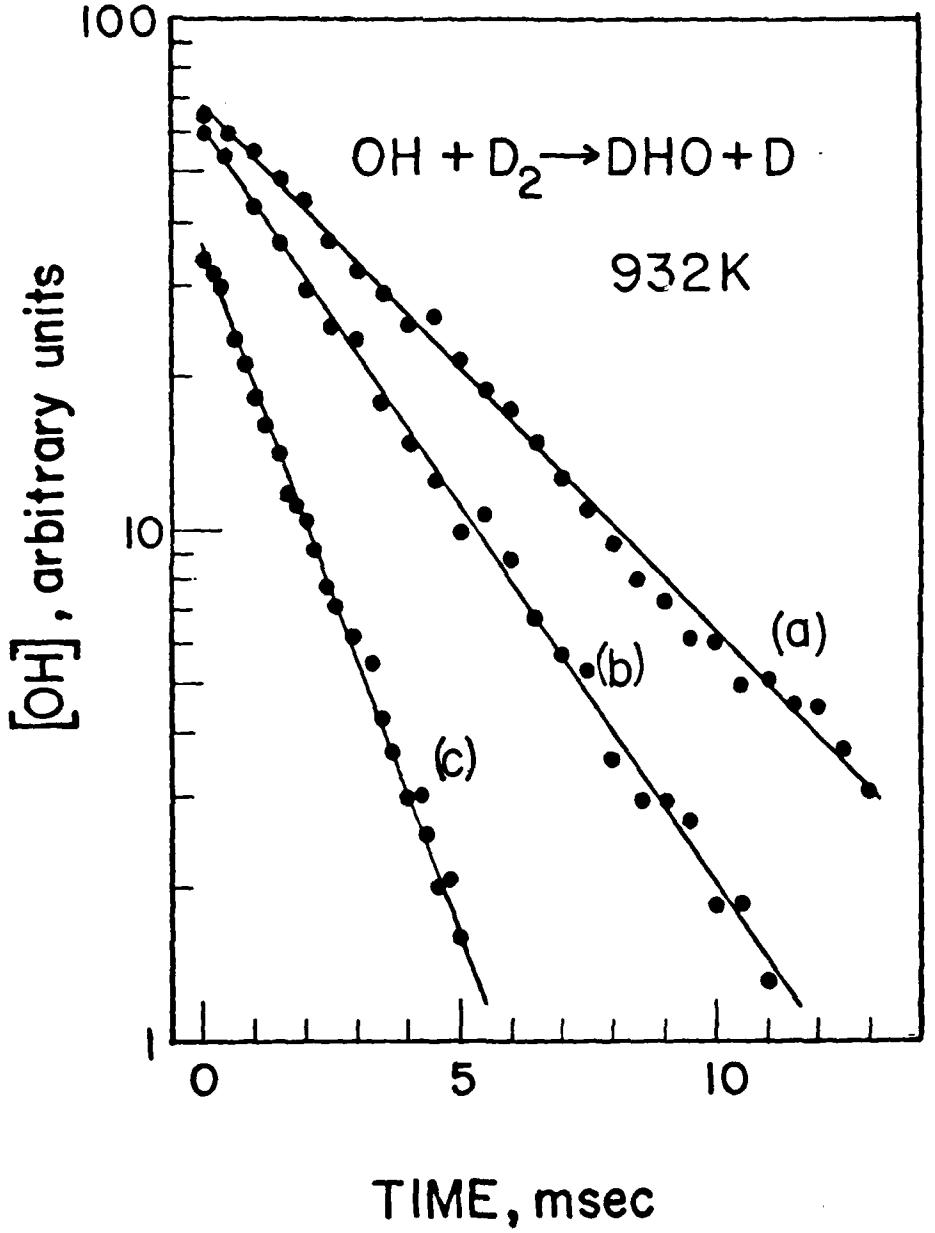
100
10
1
0
5
10
OH + D2 → DHO + D
932K
(a)
(b)
(c)
[OH], arbitrary units
TIME, msec

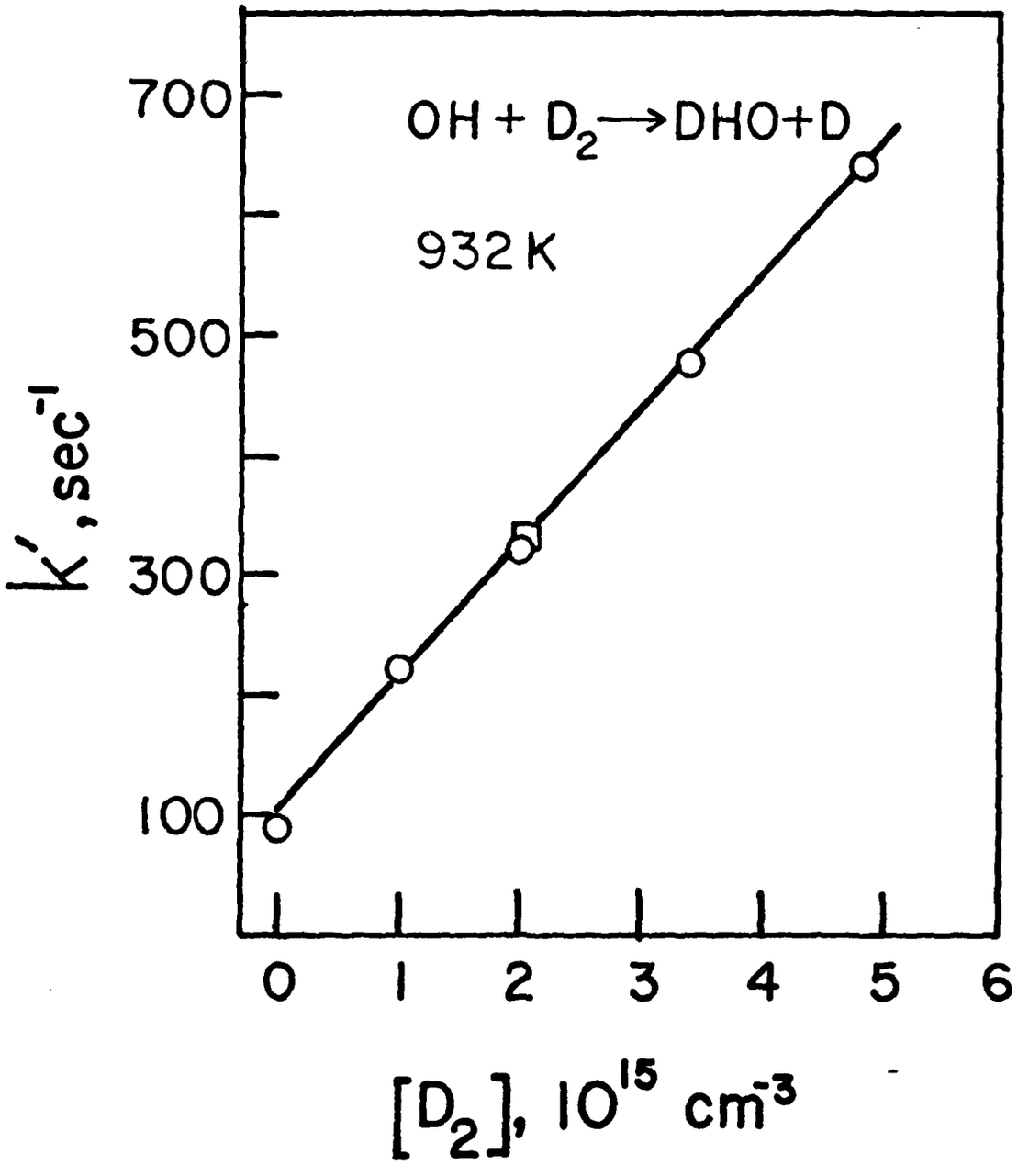
OH + D2 → DHO+D
932 K
700
500
300
100
k', sec-1
0
1
2
3
4
5
6
[D2], 10^15 cm^-3

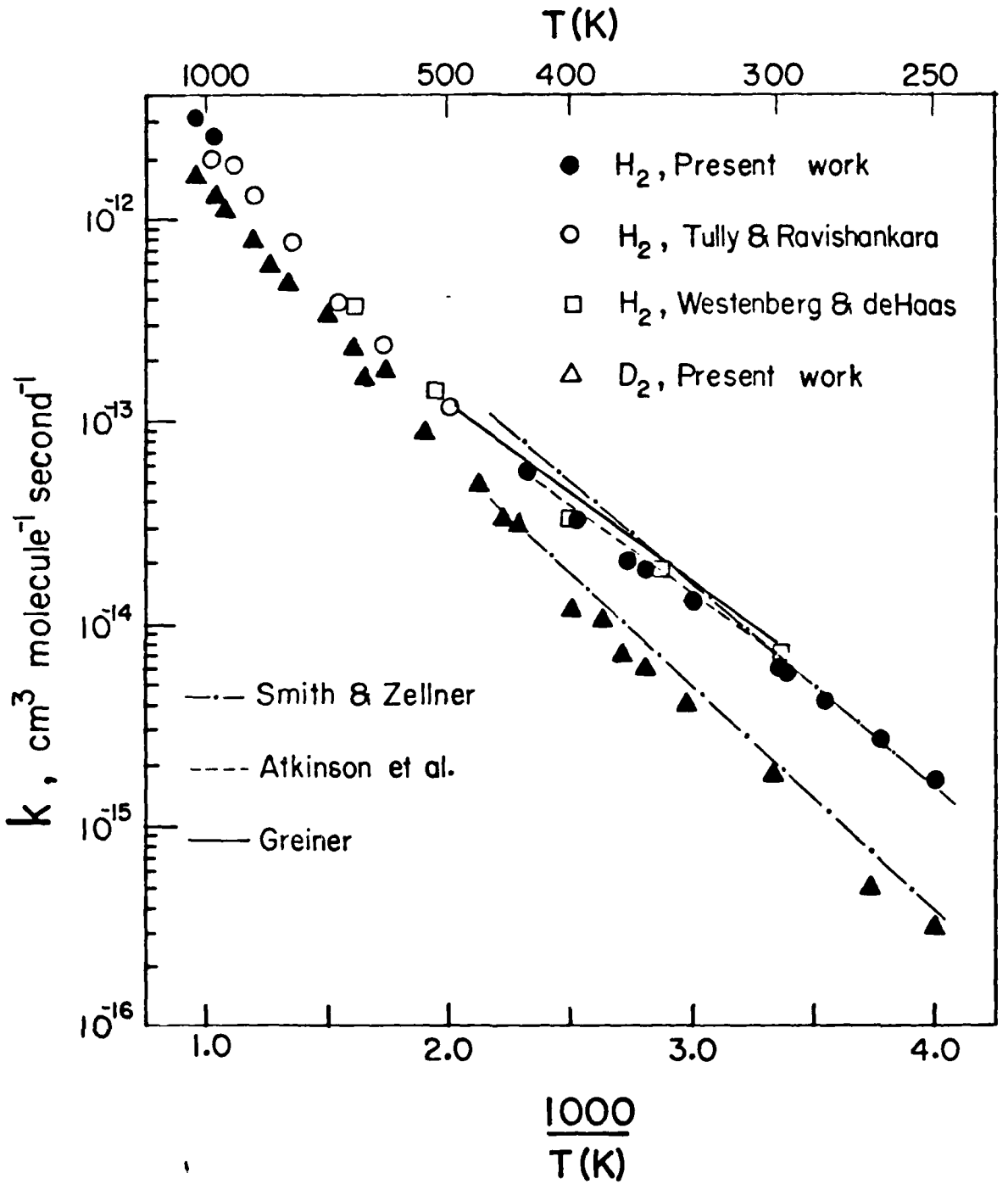
T(K)
1000
500
400
300
250
10^{-12}
10^{-13}
10^{-14}
10^{-15}
10^{-16}
k , cm^3 $molecule^{-1}$ $second^{-1}$
H_2, Present work
H_2, Tully & Ravishankara
H_2, Westenberg & deHaas
D_2, Present work
Smith & Zellner
Atkinson et al.
Greiner
1.0
2.0
3.0
4.0
1000/T(K)

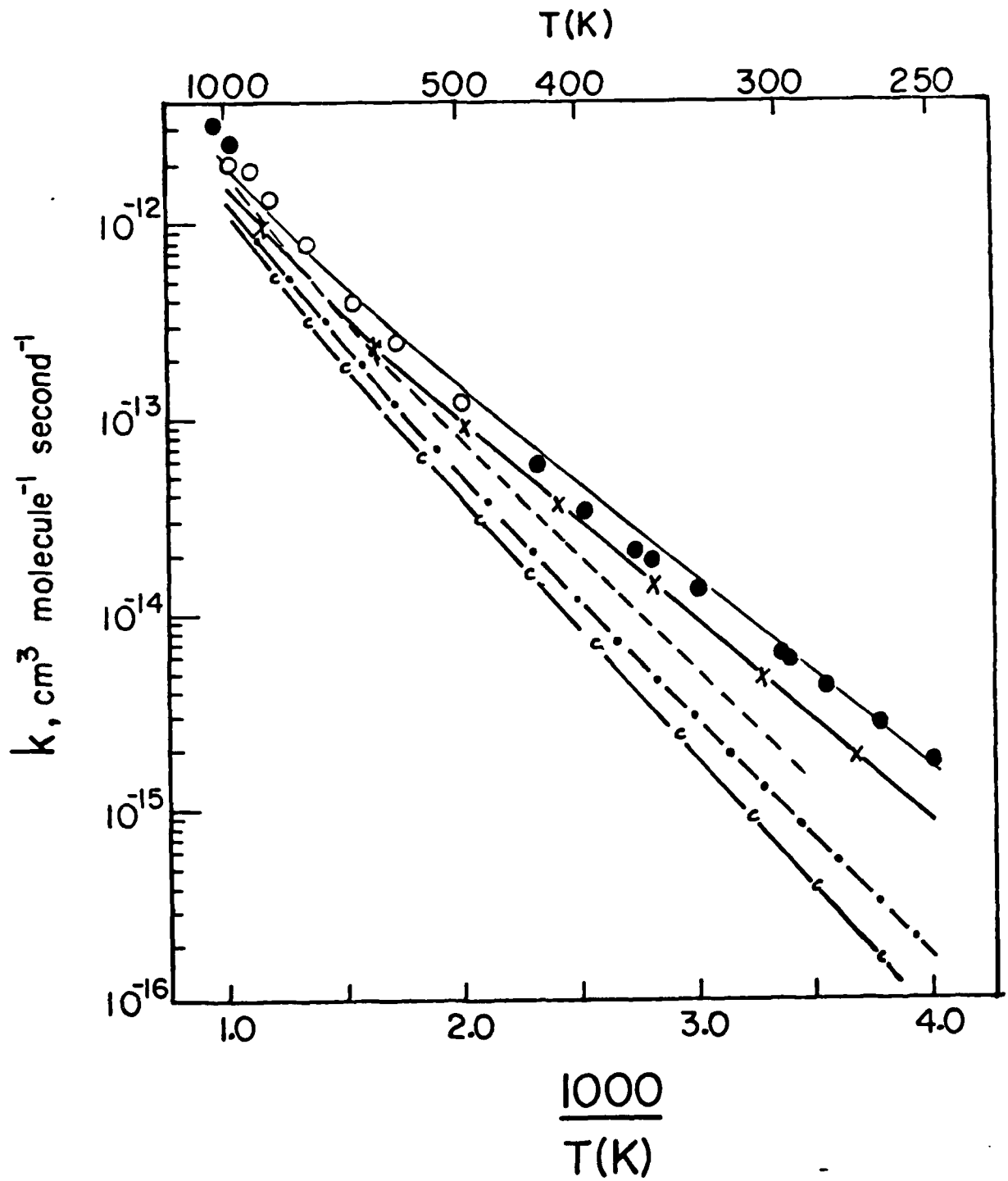
T(K)
1000
500
400
300
250
10^{-12}
10^{-13}
10^{-14}
10^{-15}
10^{-16}
k, cm^3 $molecule^{-1}$ $second^{-1}$
1.0
2.0
3.0
4.0
1000/T(K)

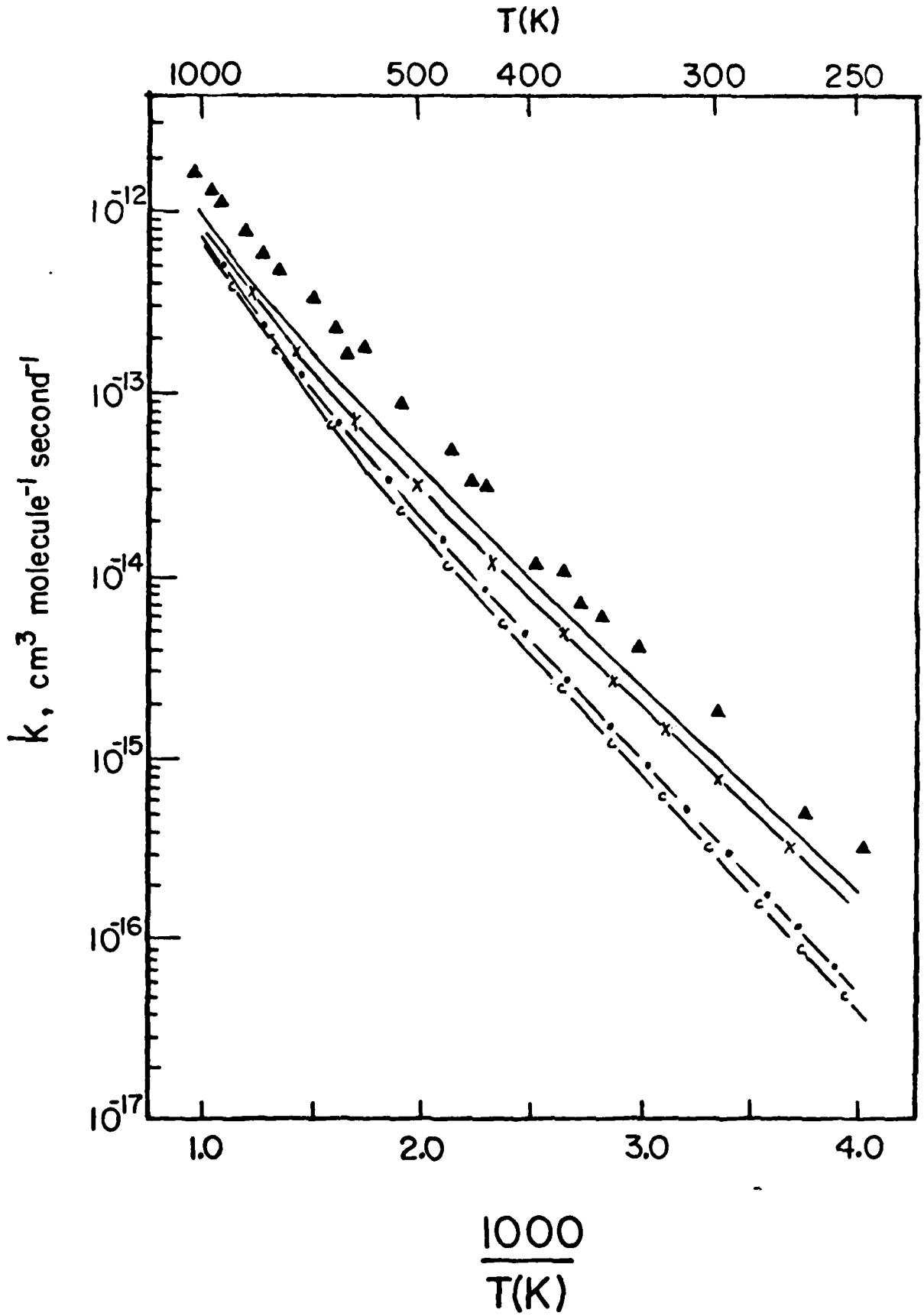
T(K)
1000
500
400
300
250
10^{-12}
10^{-13}
10^{-14}
10^{-15}
10^{-16}
10^{-17}
k, cm^3 molecule^{-1} second^{-1}
1.0
2.0
3.0
4.0
1000/T(K)

IV. KINETICS OF THE OH REACTIONS WITH CO, HCl, C_2H_6 AND C_3H_8

The reaction of hydroxyl radicals with CO,

$$OH + CO \rightarrow CO_2 + H \qquad (1)$$

is of extreme importance in combustion and atmospheric processes. In combustion systems, Reaction (1) is the principal mode of conversion of CO to CO_2. Since this reaction is very exothermic, its kinetics considerably impact the time profile for combustive energy release, and thereby, factors such as ignition, acceleration and propogation of flames. Also, in the atmosphere, Reaction (1) is the principal $CO \rightarrow CO_2$ conversion pathway; its kinetics thus impact numerous important atmospheric chemical cycles (e.g., $NO \rightarrow NO_2$).

The reaction

$$OH + HCl \rightarrow H_2O + Cl \qquad (2)$$

is one of the major pathways by which HCl is destroyed in plumes and in the stratosphere. The reactions

$$OH + C_2H_6 \rightarrow C_2H_5 + H_2O \qquad (3)$$

and

$$OH + C_3H_8 \rightarrow C_3H_7 + H_2O \qquad (4)$$

are important in hydrocarbon oxidation.

As in the case of $OH + H_2$ and $OH + CH_4$ reactions, there is a sparsity of kinetic data on Reactions (1) and (4) over the relevant combustion and plume temperatures. Therefore, k_1-k_4 were measured in the temperature range of 250-1000 K.

Experimental

The experimental technique of flash photolysis resonance fluorescence described in detail in Chapter I and III were used to carry out these measurements.

CO, HCl, C_2H_6, and C_3H_8 were obtained from Matheson Gas Products. They had the following purity levels: CO, 99.99%; HCl, >99.99%; C_2H_6, >99.96%; and C_3H_8, >99.99%. CO was passed through a liquid nitrogen trap before use. HCl, C_2H_6, and C_3H_8 were subjected to degassing cycles before use.

Results and Discussion

Experimental measurements of $k_1(T)$ for Reaction (1) are listed in Table I and plotted in Figure 1. As seen from figure 1, the curvature in the Arrhenius plot is quite dramatic. At low temperatures, the activation energy for this reaction is near zero; at higher temperatures, $k_1(T)$ increases rapidly with temperature. [It is worth noting here that visual comparisons of the 'degree' of curvature in Arrhenius plots for several reactions can be misleading; for a reaction where the low-temperature rate constant itself depends strongly on temperature, e.g., $OH + CH_4 \rightarrow H_2O + CH_3$, substnatial high-temperature rate constant enhancement may be perceived as only moderate curvature.] As in our studies of OH reactions with H_2 and CH_4, our measurements of $k_1(T)$ fill the gap between 500K and 1000K and verify the adequacy of the empirical forced fit expression of Baulch, et al. Our measurements of $k_1(T)$ above 900K lie slightly above the solid line in Figure 1; it would be worthwhile to remeasure and extend $k_1(T)$ to the 1200K temperature regime.

Rate coefficient data for Reaction (2) are listed in Table II and plotted in Figure 2. Again, the ℓnk_2 vs. 1/T plot is non-linear. The argeement between previous low-temperature (T < 298K) measurements and present results are excellent. However, it is clear that extrapolation of low-temperature data to higher temperatures would lead to large errors.

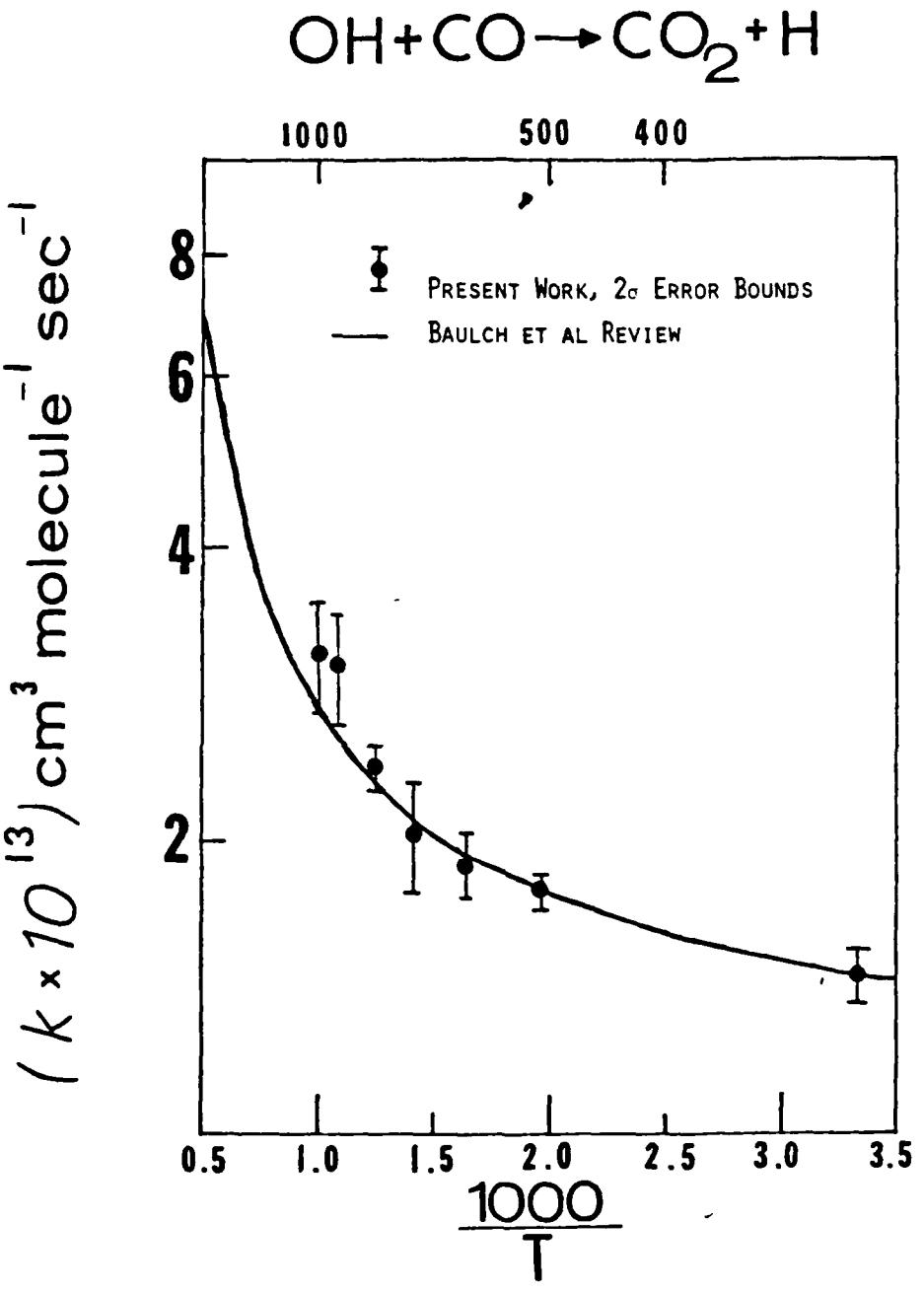

Figure 1. Plot of $\ell n k_1$ vs. $\frac{1000}{T}$.

— D.L. Bauch, D.D. Drysdale, J. Duxbury, and S. Grant, Evaluated Kinetic Data for High Temperature Reactions, Vol. 3, Butterworths, London, p. 203-249.

Table I. Rate Constant Data for the Reaction of OH with CO.

Temperature (K)	$k_1 \times 10^{13}$, $cm^3 molecule^{-1} s^{-1}$
298	1.45 ± 0.10
511	1.77 ± 0.08
607	1.89 ± 0.15
703	2.03 ± 0.26
800	2.39 ± 0.12
922	3.04 ± 0.40
992	3.11 ± 0.40

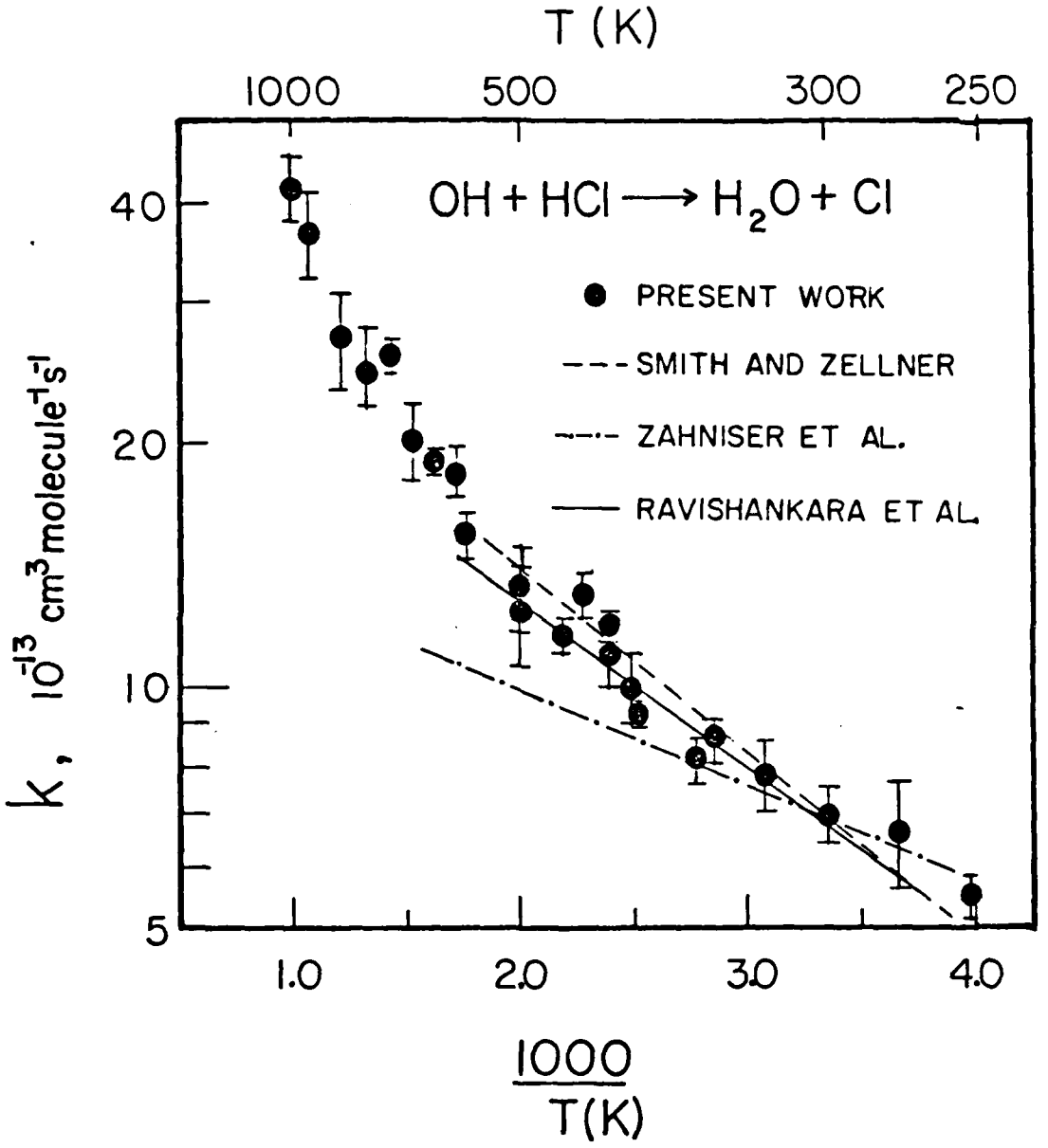

Figure 2. Plot of $\ell n k_2$ vs. $\frac{1000}{T}$.

---- I.W.M. Smith and R. Zellner, JCS Far. Trans. II, 70, 1045 (1974).

-·-·- M. Zahniser, J. Anderson, and F. Kaufman, Chem. Phys. Lett. 27, 507 (1974).

——— A.R. Ravishankara, G. Smith, Watson, and D.D. Davis, J. Phys. Chem. 81, 2220 (1977).

Table II.. Rate Constant Data for the Reaction of OH with HCl.

Temperature (K)	$k_2 \times 10^{12}$, $cm^3 molecule^{-1} s^{-1}$
252	0.553 ± 0.036
273	0.656 ± 0.098
298	0.693 ± 0.051
300	0.645 ± 0.050
328	0.787 ± 0.083
350	0.850 ± 0.059
357	0.817 ± 0.054
396	0.930 ± 0.016
402	1.09 ± 0.10
416	1.21 ± 0.05
438	1.32 ± 0.07
454	1.15 ± 0.06
500	1.33 ± 0.16
568	1.56 ± 0.08
576	1.85 ± 0.12
617	1.88 ± 0.06
656	2.03 ± 0.22
698	2.58 ± 0.10
752	2.48 ± 0.22
824	2.69 ± 0.38
932	3.63 ± 0.46
1000	4.14 ± 0.37

Rate constant data for Reactions (3) and (4) are tabulated in Table III and IV and plotted in Figures 3 and 4. Prior to these measurements, the only reliable rate constants existing for this reaction were a few measurements at and slightly above room temperature. Once again, it can be seen from Figures 3 and 4 that straight-line extrapolation of low-temperature measurements results in an underestimation of the bimolecular rate constants at higher temperatures; concave upward curvature is agin evident.

The chemical kinetics experiments described above represent valuable new input to current models of hydrocarbon combustion processes. Reactions (1) is of such fundamental importance to hydrocarbon oxidation chains that accurate characterization of these $k_1(T)$ functions is, in itself, a goal of considerable significance. Kinetic estimates for Reactions (1), (3), and (4) pervade hydrocarbon combustion modeling efforts; use of incorrect input could modify the bulk observable results of a simulated model process to an extent which implies that the assumed model structure is wrong—this may be the case, or the problem could be in the inaccuracy of the data base.

Yet one should not assume that the value of these results (and of our developed experimental technique) is limited to the numerical achievements detailed above. Typically, the complexity of the chemistry involved in a combustion and/or plume process is nearly overwhelming. In recent years it has become increasingly obvious that it is simply not possible to measure the kinetic parameters for all contributing elementary reactions in a complex process. Indeed, if such a data base did exist, computational limitations would prevent its full utilization. Increasing attention is thus being focused on the generation of 'global' kinetic equations, i.e., kinetic expressions which are approximately applicable to famililes of analogous chemical reactions. Such a viewpoint then argues the need for investigations

Table III. Rate Constant Data for the Reaction of OH with C_2H_6.

Temperature (K)	$k_3 \times 10^{12}$, $cm^3 molecule^{-1} sec^{-1}$
297	0.259 ± 0.021
400	0.771 ± 0.076
499	1.58 ± 0.10
609	2.61 ± 0.33
697	3.65 ± 0.25
800	5.07 ± 0.34

Table IV. Rate Constant Data for the Reaction of OH with C_3H_8.

Temperature (K)	$k_4 \times 10^{12}$, $cm^3 molecule^{-1} s^{-1}$
298	1.05 ± 0.04
326	1.48 ± 0.06
378	2.51 ± 0.20
469	3.37 ± 0.23
554	4.78 ± 0.34
690	8.78 ± 0.97

$$OH + C_2H_6 \rightarrow H_2O + C_2H_5$$

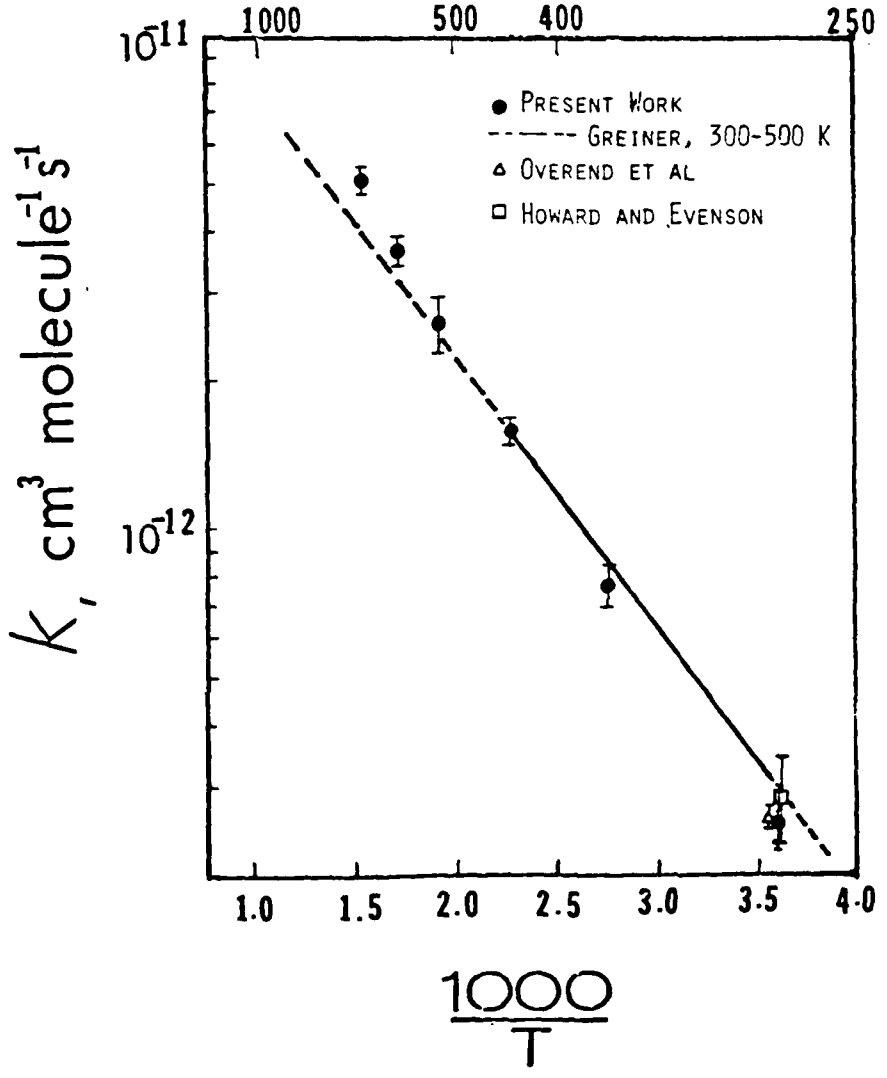

Figure 3. Plot of $\ell n k_3$ vs. $\frac{1000}{T}$.

----- N.R. Greiner, J. Chem. Phys. 53, 1070-76 (1970).
△ R. Overend, G. Paraskevopoulos, and R. J. Cvetanovic, Can. J. Chem. 53, 3374-3382 (1975).
□ C.J. Howard and K.M. Evenson, J. Chem. Phys. 64, 4303-4306, (1976).

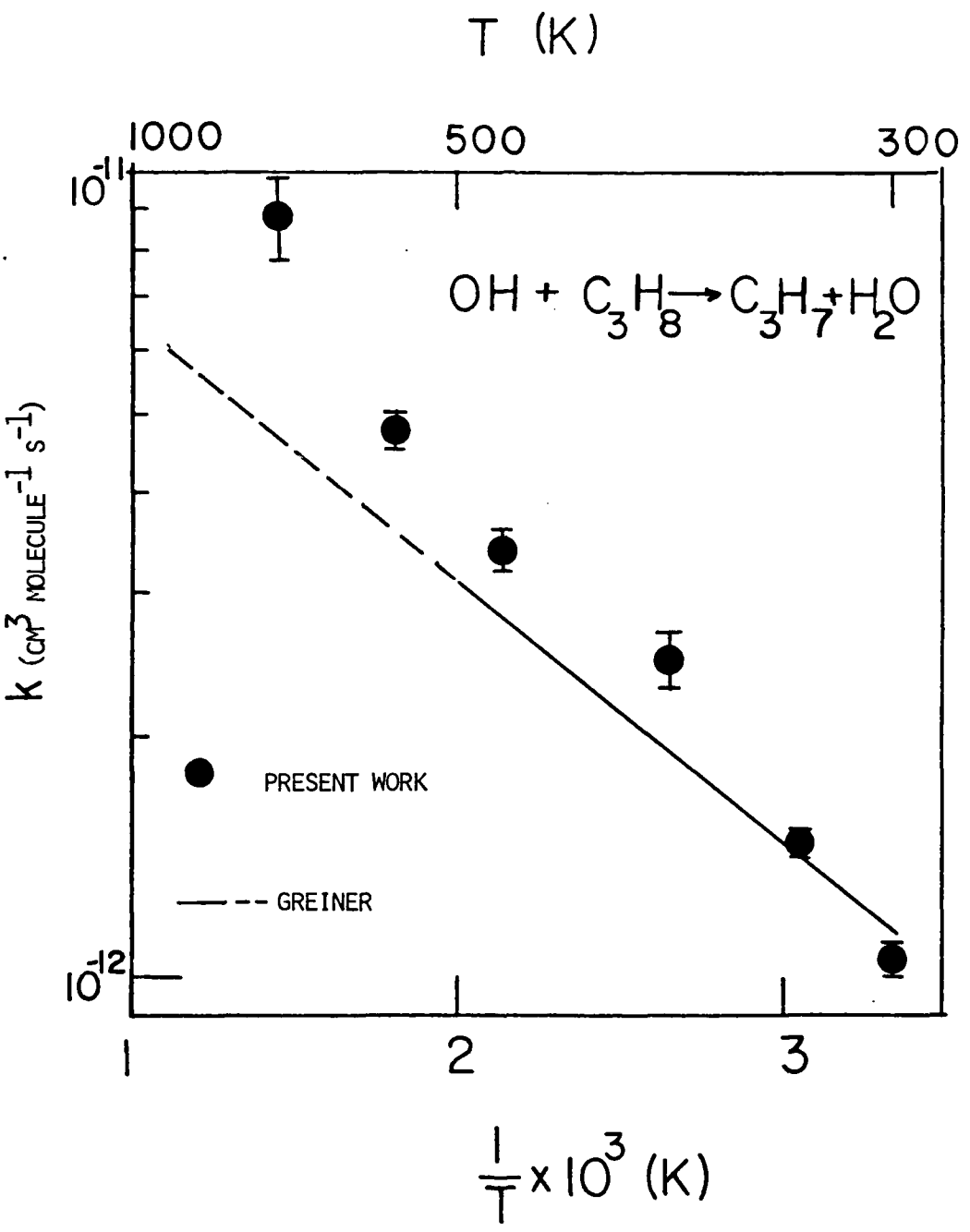

Figure 4. Plot of $\ell n k_4$ vs. $\frac{1000}{T}$.

— N.R. Greiner, J. Chem. Phys. 53, 1970 (1970).

which emphasize the effects of chemical structure on the rates of reactivity; studies aimed at generating an improved understanding of the general temperature dependence of bimolecular reaction rates must be pursued.


DATE
ILME